International Journal of Informatics Society

11/24 Vol.16 No.2 ISSN 1883-4566

Informatics Society

Aims and Scope

The purpose of this journal is to provide an open forum to publish high quality research papers in the areas of informatics and related fields to promote the exchange of research ideas, experiences and results.

Informatics is the systematic study of Information and the application of research methods to study Information systems and services. It deals primarily with human aspects of information, such as its quality and value as a resource. Informatics also referred to as Information science, studies the structure, algorithms, behavior, and interactions of natural and artificial systems that store, process, access and communicate information. It also develops its own conceptual and theoretical foundations and utilizes foundations developed in other fields. The advent of computers, its ubiquity and ease to use has led to the study of informatics that has computational, cognitive and social aspects, including study of the social impact of information technologies.

The characteristic of informatics' context is amalgamation of technologies. For creating an informatics product, it is necessary to integrate many technologies, such as mathematics, linguistics, engineering and other emerging new fields.

Guest Editor's Message

Fumiaki Sato

Guest Editor of the Forty-seventh Issue of the International Journal of Informatics Society

We are delighted to have the Forty-seventh issue of the International Journal of Informatics Society (IJIS) published. This issue includes selected papers from the Sixteenth International Workshop on Informatics (IWIN2023), held online from September 1st – 4th, 2023. The workshop was the seventeenth event for the Informatics Society. It was intended to bring together researchers and practitioners to share and exchange their experiences, discuss challenges and present original ideas in all aspects of informatics and computer networks. In the workshop, 27 papers were presented in six technical sessions. The workshop was successfully finished, and precious experiences were provided to the participants. It highlighted the latest research results in informatics and its applications, including networking, mobile ubiquitous systems, data analytics, business and industrial systems, education systems, design methodology, intelligent systems, groupware, and social systems, etc.

Each paper submitted to IWIN2023 was reviewed in terms of technical content, scientific rigor, novelty, originality, and presentation quality by at least two reviewers. Through those reviews, 22 papers were selected for publication candidates of the IJIS Journal, and they were further reviewed as Journal papers. We have three categories of IJIS papers, Regular papers, Practical papers, and Invited papers, each of which was reviewed from different points of view. This volume includes papers among those accepted papers, which have been improved through the workshop discussion and the reviewers' comments.

We publish the journal in print as well as in an electronic form over the Internet. We hope that the issue would be of interest to many researchers as well as engineers and practitioners all over the world.

Fumiaki Sato received his BE from Iwate University in 1984. He received his ME from Tohoku University in 1986. He joined Mitsubishi Electric in the same year. He obtained his Ph.D. in Engineering from Tohoku University in 1992. He became an associate professor at the Faculty of Engineering, Shizuoka University, in 1995. He became a professor at the Faculty of Science, Toho University, in 2005. He is involved in the research and development of formal specification description languages, communication protocol testing and verification, distributed processing systems, and mobile computing. He served as the secretary and workshop chairman of the Information Processing Society of Japan DPS Study Group. He is currently a senior member of the Information Processing Society of Japan, a member of the Institute of Electronics, Information and Communication Engineers, IEEE, and ACM.

Regular Paper

Applying Two-Dimensional Trust Representations to Supporting University Students' Job Hunting — a Case Study with the Non-Cumulative Distrust Levels

Yoshinobu Kawabe† and Tetsuhisa Oda†

†Graduate School of Business Administration and Computer Science, Aichi Institute of Technology, Japan
{kawabe, oda}@aitech.ac.jp

Abstract - In recent years, it has been an important research topic in information security to evaluate the trustworthiness of information. The theory of trust computation deals with trustworthiness as a computational object, enabling us to infer and predict the reliability of information. We have proposed a new method for trust computation, which employs a two-dimensional trust degree that handles trust and distrust simultaneously. We have shown that this method is an extension of Marsh et al.'s well-known one-dimensional trust value method, and our approach is an extension of Jøsang's Subjective Logic. In that sense, our previous results show the technique with a two-dimensional trust value is powerful enough from a theoretical point of view. However, it needs to be clarified how to apply our trust values to real problems. In this paper, we conduct a large-scale case study using two-dimensional trust values. Specifically, we work on a case study of developing a recommender system for employment opportunities that match those based on university students' employment preferences. In our case study, students can answer desired and undesired items as text in an open-ended response format. After analyzing the text, we calculate a trust value, representing an agreement between the student's preferences and the company profile. Since students describe desirable and undesirable items independently and maybe inconsistently, leading to difficulty coping with the inconsistency. Our trust value can deal with this inconsistency, and we determine a trust value without inconsistency by applying the result from the fuzzy logic. This paper also discusses how to assess trust and distrust levels. We show and validate our criteria by comparing them with those in another case study of deciding a trust value to rescue requests posted in a disaster.

Keywords: On-Line Trust, 2D Trust Model, Fuzzy Logic, Job Placement Assistance

1 INTRODUCTION

In recent years, techniques for evaluating trustworthiness in information and senders/receivers are getting crucial. Marsh et al. proposed a method to deal with trustworthiness as a computational object, but their approach has a problem in that it could not handle the independence of trust and distrust degrees. To overcome this problem, we extended Marsh et al.'s trust computation method with the fuzzy logic-based FCR method [1,2]. Our trust computation is two-dimensional, where we can deal with trustworthiness and distrust-worthiness independently. Our previous work [3, 4] has introduced a two-dimensional trust representation, and we have also shown how to analyze transition-related trust properties, such as safety properties. However, we still need to give how to determine the specific trustworthiness and distrust-worthiness when applying our extended trust model to real problems. This paper examines how to determine trust and distrust levels through a case study.

This paper, specifically, deals with a method for recommending companies that match the job preferences of university students based on their job preferences. University students' main interests regarding companies they are employed by are the type of job and workplace location. In this study, we asked university students to answer "what they want" and "what they do not want" regarding these conditions in the form of free descriptions, and based on the results, we calculated a two-dimensional trust value of [3, 4].

Since students tend to describe their preferences and non-preferences independently, the requirements of college students regarding corporate profiles may be inconsistent. We computed the net goodness of fit (called a one-dimensional trust value) of students' preferences to the company profile using the integrated value of the FCR method.

In this study, the assignment of the degree of trust and the degree of distrust was conducted using the same approach as in our previous study, the assignment of a two-dimensional trust value to rescue requests posted during a flood disaster [5]. Specifically, trustworthiness is determined by the degree of compatibility between the text of the company profile and the student's expectations and is a value between 0 and 1. On the other hand, the distrust level is assigned based on whether or not the student's "undesired items" appear in the company profile and has a value of 0 or 1. Although it is possible to determine the distrust level based on "how many unwanted items appear" using the same criterion as the trust level, we did not do so in this study. To validate the criterion of this paper, we discuss how to determine the distrust level properly.

2 PRELIMINARIES: TWO-DIMENSIONAL TRUST REPRESENTATIONS

Marsh and Dibben introduced trust values, which range from -1 to 1, and classified trust notions into *trust*, *distrust*, *untrust*, and *mistrust* [6]. We extended their trust values for two dimensions [3,4] to address inconsistent trust evaluations. This section explains some basics of (mainly two-dimensional) trust computations.

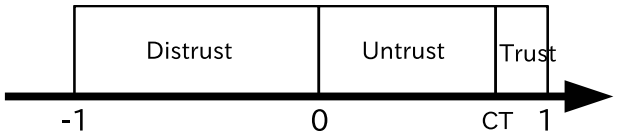

Figure 1: Marsh's trust model

2.1 Conventional Trust Values

A conventional trust value is a real number in $[-1, 1)$. Readers interested in the details of calculating trust values can find them here [6], but in this paper we directly handle the calculated trust values. Marsh and Dibben introduced the following four notions of trust (see also, Fig. 1):

- *Trust*: The notion represents a case where a trust value is positive and exceeds a predefined value called a cooperation threshold (CT). In this case, a trustee should be trusted, and the trust value is regarded as a measure of how much an agent believes the trustee.
- *Distrust*: Here the trust value is negative, and an agent believes that a trustee will actively work against her in a given situation.
- *Untrust*: Although the trust value is positive, it is not high enough to produce cooperation. An agent cannot determine if a trustee is actually trustworthy.
- *Mistrust*: Initial trust has been betrayed. More precicely, mistrust represents a situation either a former trust was destroyed or a former distrust was healed. The mistrust notion is a time-related trust property.

For these properties, see studies by Primiero [7] (on distrust and mistrust) and [8] (on trust and distrust).

2.2 Fuzzy-Logic-Based Two-Dimensional Trust Values

Marsh and Dibben classified trust notions in a one-dimensional setting, i.e., trust and distrust are at both extremities. However, Lewicki et al. [9] suggested that trust and distrust are entirely different dimensions from a psychological viewpoint. Trust is a property closely related to human impressions, and a technique for impression formation based on mathematical psychology should be applied to trust values.

Oda [1, 2] developed a Fuzzy-set Concurrent Rating (FCR) method with fuzzy logic that enables us to measure and analyze human impressions. The FCR method allows two or more dimensions for representing a truth value, and our two-dimensional trust representation is an application of the FCR method for trust and distrust notions.

2.2.1 FCR Method

The FCR method employs the Hyper Logic Space model (HLS) as a logic space for multiple-dimensional multiple-valued logic. Figure 2 shows a two-dimensional space based on $true$ and

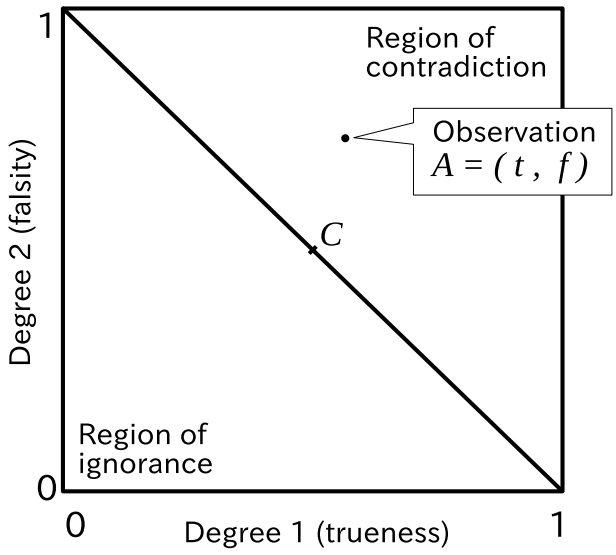

Figure 2: Two-dimensional HLS

$false$. For any $t, f \in [0, 1]$, pair (t, f) is called an observation. t and f are independent; we do not assume such conditions as $t + f = 1$. We call $\{(t, f) \,|\, t, f \in [0, 1] \wedge t + f > 1\}$ the region of contradiction. $\{(t, f) \,|\, t, f \in [0, 1] \wedge t + f < 1\}$ is called the region of ignorance, or the region of irrelevance. Finally, $\{(t, f) \,|\, t, f \in [0, 1] \wedge t + f = 1\}$ is the consistent region.

Given observation (t, f), we need to calculate an actual truth value, which is called an integration value. Integration values can be calculated in several ways, and we employ the reverse-item averaging method, where integration value I_2 is defined with $I_2(t, f) = \dfrac{t + (1 - f)}{2}$. The integration value is the average of the degree of the positive elements and the complementary degree of the negative elements.

Another important value in the FCR method is the degree of contradiction [1,2] or the contradiction-irrelevance degree. In the field of personality psychology, some situations are allowed, including "I like it, but I don't like it" or "I don't care for it at all." The degree of such confusion/irrelevance is formulated with the degree of contradiction. For observation (t, f), degree of contradiction $C(t, f)$ should satisfy $C(t, f) = 1$ for complete confusion, $C(t, f) = -1$ for complete ignorance, and $C(t, f) = 0$ for a consistent situation. $C(t, f) = t + f - 1$ is usually employed where $C(t, f)$ represents the distance between (t, f) and the consistent region.

2.2.2 Two-Dimensional Trust Model

We employ the degrees of trust $Trust$ and distrust $DisTrust$ defined with $Trust = DisTrust = \{\, v \,|\, 0 \leq v \leq 1\}$ and define a two-dimensional trust value as an element of $Trust \times DisTrust$. Observation $(1, 0) \in Trust \times DisTrust$ has a high degree of trust and a low degree of distrust and represents a case where a trustee is completely trusted; this observation corresponds to trust value 1 of [6]. Observation $(0, 1)$ represents a case of complete distrust and corresponds to trust

value -1. Observation $(0.5, 0.5)$, which falls exactly between $(1, 0)$ and $(0, 1)$, corresponds to 0 in conventional trust values.

To define such trust notions as trust, distrust, and untrust in our two-dimensional trust model, we employ the following transformation:

$$\left[\begin{pmatrix}\cos\frac{\pi}{4} & -\sin\frac{\pi}{4}\\ \sin\frac{\pi}{4} & \cos\frac{\pi}{4}\end{pmatrix}\left\{\begin{pmatrix}t\\ d\end{pmatrix}-\begin{pmatrix}1\\ 0\end{pmatrix}\right\}+\begin{pmatrix}\frac{\sqrt{2}}{2}\\ 0\end{pmatrix}\right]\times\frac{1}{\frac{\sqrt{2}}{2}}$$
$$=\begin{pmatrix}t-d\\ t+d-1\end{pmatrix}=\begin{pmatrix}i\\ c\end{pmatrix}.$$

First element $i = t-d$ can be calculated with the reverse-item averaging method. Actually, the value of i is calculated by normalizing $I_2(t, d)$ to be a value in region $[-1, 1]$; note that the range of integration value $I_2(t, d)$ was originally $[0, 1]$.

The value of i was regarded as a conventional trust value given by Marsh and Dibben. From the definition of $i = t - d$, a net trust value is calculated by subtracting the degree of trust from the degree of distrust, which matches our intuition. In Fig. 2, the consistent region is the line between $(1, 0)$ and $(0, 1)$ and corresponds to the set of conventional trust values. Observation (t, d) in the consistent region satisfies $t + d = 1$ and is regarded as an assumption on the trust and distrust degrees. The theory of conventional trust values implicitly introduces this assumption.

Trust notions are defined with the value of i. Let CT be a cooperation threshold. If we have $i = t - d \geq CT$, then it is a case of trust; if i is negative then it is case of distrust; if we have $0 \leq i < CT$, then it is a case of untrust. Note that for the case of distrust, condition $i < 0$ is equivalent to $t < d$; i.e., a trustee is distrusted if the degree of distrust exceeds the degree of trust.

As described above, the i value in our two-dimensional trust model corresponds to Marsh's trust value. Thus, our model is an extension of the one-dimensional model. Moreover, our model is also an extension of Jøsang's Subjective Logic [10]. Subjective Logic, like our model, treats trustworthiness t and distrustworthiness d independently. However, Subjective Logic requires the constraint $t + d \leq 1$. The trust model based on the FCR method has no such constraint. Therefore, our model is an extension of Subjective Logic in that it can handle t and d with $t + d > 1$.

3 CALCULATION OF TWO-DIMENSIONAL TRUST VALUES BASED ON MATCHING OF EMPLOYMENT PREFERENCES AND JOB OFFERS

For applying our two-dimensional trust model to real applications, this section deals with the issue of helping university students find jobs using our two-dimensional trust values. Specifically, we evaluate the degree to which a description in job openings matches the student's preferences as a two-dimensional trust value.

This study focuses on students in the Department of Information Science at Aichi Institute of Technology. Although the students are in the sciences, the percentage of students going to graduate school is about 20%, and most undergraduates wish to find a job. Readers should note that this is a different characteristic from that of students at national universities in Japan. However, private university students account for 70% of the total students in Japan, and we believe that students with this characteristic are not a minority. About 80% of the students commute from the Tokai region of Japan. The general trend is that they are strongly oriented toward the IT industry and hope to live in their hometown (i.e., they wish to work in the Tokai region). The number of job openings is about 15,000, mainly for engineering students. In this section, we focus on the example of one student, but we treated 78 job-seeking students.

```
Preferred items regarding work location:
I prefer to work and live in Nagoya or
Tokyo.  It is also OK to work in my home
town Hamamatsu.

NG items regarding work location:
I'm not particularly eager to go to
outlying areas such as Hokkaido, Okinawa,
and Shikoku.

Preferred occupations:
I am considering IT sales, planning,
other sales jobs, financial institutions,
and recruiting services.

NG Occupations:
I have no NG occupations.
```

Figure 3: Description of one student's wishes

Note that the primary purpose of this case study is to provide students with a list of company information, and we do not aim to automatically find a company that fully matches the student's preferences. Our tool lists multiple companies, which our technique extracts from 15,000 job postings; many of the students targeted in this study could be better at this extraction process and need help with a tool. The tools in this study will help assist such students with job placement guidance. We believe the tool that allows students to be presented with a list of potential companies through a short interview was useful.

3.1 Preprocessing: Extracting Workplace Locations and Job Types

We first obtained information from the students on their "preferences" and "things to avoid" about work location and job type. This information was obtained through open-ended questions; we show an example of the result in Fig. 3.

We use the morphological analyzer MeCab [11] to extract words related to place names and occupations. Then, we conduct a keyword search to find a match between the company profile text and student preferences.

To find a better match, after extracting proper nouns, such as the region's name, we add information on neighboring areas, considering the characteristics of the target student's preferences; especially, note that students like to get a job on

- XXX Corporation
  - **Tokyo**, Sendai, **Nagoya**, Osaka, Hakata, and 40 other locations. Miyagi, **Tokyo**, Nagano, **Aichi** (**Nagoya**), Osaka, and Fukuoka
  - Software, **Information** Processing, and **Information** **Services**. Development, sales, and maintenance of office equipment (**information** processing equipment) and systems. Listed on the first section of the Tokyo Stock Exchange. Flextime system available (core hours: 11:00-15:00). Telework system available. Clients include government agencies, **financial** institutions, etc.
  - **Sales jobs**, system engineers, customer engineers, technical staff, development, and research staff. A driving license is required for some positions.
  - (The rest of this job offer contains information on capitalization, annual sales, etc.)

Figure 4: Example of job opening

local orientation toward the Tokai region. For example, if the student wishes to work in "Nagoya," the neighboring districts "Aichi" and "Owari" are also used as keywords for the search. Similarly, in Fig. 3, the student has listed Hokkaido, Okinawa, and Shikoku as their least preferred work regions. These are not exact names of regions but rather broad regional names. Most of the place names in the job openings (typically, location of branch offices, factories, etc.) are city names. Therefore, for the three words "Hokkaido, Okinawa, and Shikoku," we will also add more detailed place names within the regions for matching, such as "Ehime, Asahikawa, Kagawa, Takamatsu, Kochi, Sapporo, Muroran, Matsuyama, Tokushima, Naha, Hakodate, and Kitami."

In finding a better match on job categories, because target students major in information technology, some search words are added before searching. For example, when "IT" appears in the description of desired items, the term "information" is also used.

On the other hand, to conduct a job matching, we created a dictionary with job information based on the information in the job posting, as shown in Fig. 4; such a posting contains information such as the location of the head office, the place of work, and the text of the company profile. In the example in Fig. 4, we underline the occurrence of words that match the student's desired information described above.

3.2 Calculating Two-Dimensional Trust Values

In this study, we calculated the degree to which words from the student's preferences appeared in the job postings for each work location and job type. For example, in the above case, the evaluation values are as follows[1]:

- The matching degree of location preference is 0.6; actually, 3 out of 5 words "Aichi, Tokyo, Owari, Hamamatsu, and Nagoya" as matching candidates match the job information; and
- The match level for job type is 0.8; 4 out of 5 possible matching words "information, sales, finance, recruiting, and service" match the job information.

In this study, we used the goodness of fit as trust values concerning the work location or the type of job. The trust level is the degree to which the text of the company profile matches the positive aspects desired by the student. The value is a real number between 0 and 1.

On the other hand, the distrust level was determined by whether or not the words that the students did not want appeared in the company profile. This decision is based on the fact that students tend to avoid firms whose profile contains items the students wish to avoid. This results in a distrust level of either 0 or 1.

In Fig. 3, the student listed Hokkaido, Okinawa, and Shikoku as the least preferred work locations. For the case of this student, the level of distrust regarding the work location is determined by whether or not the name of one of the following places or regions appears in the work location field of the job opening: Ehime, Asahikawa, Okinawa, Kagawa, Takamatsu, Kochi, Sapporo, Shikoku, Muroran, Matsuyama, Tokushima, Naha, Hakodate, Hokkaido, or Kitami. For the firm shown in Fig. 4, no such place name appears in the job opening. Thus, this student's distrust level concerning this firm is 0.[2] Therefore, the two-dimensional trust value about the workplace location of this firm is $(0.6, 0)$.

In the above matching, we calculated the trust and distrust levels independently. Therefore, there may exist inconsistencies in the trust and distrust levels. For example, for the two-dimensional trust value $(0.6, 0)$ above, we can calculate the degree of the discrepancy from a consistent trust value using Oda's fuzzy logical approach; the degree is $|(0.6 + 0) - 1| = |-0.4| = 0.4$. Also, we can calculate the observation point without inconsistency with Oda's reverse-item averaging method, and the result is $(0.8, 0.2)$; note that the first element of the pair is the integration value.

One can also obtain Marsh's one-dimensional trust value from the two-dimensional trust value, considering the observation point $(0, 1)$ as Marsh's score -1 and $(1, 0)$ as score 1, respectively. We can see the one-dimensional trust level as the "net trust value" obtained by subtracting the distrust level from the trust level. From the viewpoint of fuzzy logic, a one-dimensional trust value is a trust level without the inconsistency of evaluation, corresponding to the integration value[3].

In the above example, the distrust level is 0, so the first element of the pair $(0.6, 0)$ and the corresponding one-dimensional trust value 0.6 coincide. If the job offer includes a negative statement regarding the location of the job, the trust value

[1] Although we give an example in English, we actually search for Japanese keywords.

[2] Note that the job offer form also states "40 other locations," which may include specific locations the students do not wish to work at, although it is not specified. Only text matching was used in this study, and semantic analysis was not conducted.

[3] There is a difference in that the integration value ranges from 0 to 1, while the one-dimensional trust value ranges from -1 to 1.

- XXX Corporation $(0.8, 0.6, 451)$
  - Tokyo, Sendai, Nagoya, Osaka, Hakata, and 40 other locations. Miyagi, Tokyo, Nagano, Aichi (Nagoya), Osaka, and Fukuoka
  - Software, Information Processing, and Information Services. Development, sales, and maintenance of office equipment (information processing equipment) and systems. Listed on the first section of the Tokyo Stock Exchange. Flextime system available (core hours: 11:00-15:00). Telework system available. Clients include government agencies, financial institutions, etc.
  - Sales jobs, system engineers, customer engineers, technical staff, development, and research staff. A driving license is required for some positions.
- YYY Corporation $(0.6, 0.8, 2000)$
  - Tokyo Hamamatsu, Nagoya, and Osaka. Chiba, Tokyo, Kanagawa, Shizuoka, Aichi, Kyoto, Osaka, and Hyogo.
  - System design, construction, operation, maintenance, various software development, etc. We support IT infrastructure in a wide range of industries from finance, manufacturing, telecommunications, and services to space development. We provide solutions in various phases from system development, operation, and maintenance to infrastructure construction.
  - System Engineer.
- ZZZ Corporation Nagoya Branch $(0.6, 0.8, 1219)$
  - ...

Figure 5: Output result (partly)

would be 1. In this case, the two-dimensional trust value is $(0.6, 1)$, and the Marsh trust value is negative -0.4.

Similarly, for the job type, we defined the distrust level based on whether or not the job type the student does not want appears in the job offer text. Since the student's statement in the previous section states that "I have no NG occupations," the value of the distrust level is 0. Therefore, the two-dimensional trust value for the job category is $(0.8, 0)$.

3.3 Presenting a List of Recommendable Companies

Applying the above technique, we give trust values for work locations and job types for each job posting's entry. Then, we compute one-dimensional trust values to find a match between student and company profiles. Finally, a list of 20 job openings is presented to the student. Figure 5 shows an example of the output; actually, they are in Japanese. The list of the output is sorted in the order of:

1. one-dimensional trust value for job type,
2. one-dimensional trust value for work location, and
3. the number of employees of the company.

These elements are shown as a triple placed on the right-hand side of the company name.

In this study, we implemented the recommender system on Linux (Ubuntu 22). We used a set of job data in a CSV format with approximately 15,000 entries, extracted keywords, and converted them into a form Common Lisp could handle. The conversion was conducted with a shell script, using the morphological analyzer MeCab for natural language processing. For collecting students' preferences, we used Moodle. Students can describe their preferences in a free-style text format, and we extracted keywords such as work location or occupations from the text, and the resulting keywords were given to a Lisp program. Finally, the resulting Lisp program can calculate trust values and match the student's wishes and company profiles. We used Steel Bank Common Lisp (SBCL 2.1.11) in this study.

Our recommender system has presented some job openings that may not appropriately reflect the student's preferences; for example, some job offers contain work locations in foreign countries. However, the recommender system can present a sufficiently large number of job offers, and on the whole, the system gives a list of companies that match the student's preferences.

4 CONSIDERING CRITERIA FOR DISTRUST LEVELS

In our previous work [4, 5], we determined the trust level part of a two-dimensional trust value by accumulating positive factors. This study also collects favorable aspects of a firm's job openings for the trust level part of a two-dimensional trust value; that is, we increase the trust level when keywords that match the student's expectations appear in the company profile text.

On the other hand, we can see at least two types of cases in determining the distrust level. This section discusses how to determine the distrust level.

4.1 Case 1: Cumulative Distrust Level

The first approach is to determine the distrust level based on the cumulative degree of unfavorable evaluations, similar to the method used to determine the credibility level. The following is an example in [4].

Example 1 *In three countries, an opinion poll was conducted about the approval ratings of each country's governments. We used the following items to answer this question: "Do you trust your government?"*

1. *I have no idea;*
2. *Yes, I do;*
3. *No, I do not;*
4. *Sometimes yes, sometimes no.*

The number of answers for each item is $a_1^c, \ldots, a_4^c$ for country c; also, we have $s^c = a_1^c + a_2^c + a_3^c + a_4^c$. In this example,

we calculate the degrees of trust t_c and distrust d_c of the government with $t_c = \frac{a_2^c + a_4^c}{s^c}$ and $d_c = \frac{a_3^c + a_4^c}{s^c}$. A survey was conducted with 100 residents each in the countries of X, Y, and Z, and the following are the results:

$$\begin{array}{rcl}(a_1^X, a_2^X, a_3^X, a_4^X) & = & (10, 20, 30, 40),\\ (a_1^Y, a_2^Y, a_3^Y, a_4^Y) & = & (50, 30, 10, 10),\ \textit{and}\\ (a_1^Z, a_2^Z, a_3^Z, a_4^Z) & = & (20, 25, 5, 50).\end{array}$$

For each country, we can give the degrees of trust t_c and distrust d_c as follows:

$$\begin{array}{rcl}(t_X, d_X) & = & (0.6, 0.7),\\ (t_Y, d_Y) & = & (0.4, 0.2),\ \textit{and}\\ (t_Z, d_Z) & = & (0.75, 0.55).\end{array}$$

For each country we can also calculate the one-dimensional trust value i_c and the degree of inconsistency c_c[4]*:*

$$\begin{array}{rcl}(i_X, c_X) & = & (-0.1, 0.3),\\ (i_Y, c_Y) & = & (0.2, -0.4),\ \textit{and}\\ (i_Z, c_Z) & = & (0.2, 0.3).\end{array}$$

Suppose we define the two-dimensional trust values as in the approach of this example. In that case, the value of the distrust level gradually increases as the number of responses on items *3.* and *4.* in the questionnaire increases. In this sense, the distrust level is cumulative and takes various values between 0 and 1. We can see that the distrust level reaches extremities (i.e., values around 0 or 1) when either "almost all respondents answered with item *1.* or item *2.*, and the distrust level becomes around 0" or "almost all respondents answered with item *3.* or item *4.*, and the distrust level gets higher and becomes around 1." This consideration suggests that, in general, this method of determining the distrust level is unlikely to result in extreme values.

4.2 Case 2: Non-Cumulative Distrust Level

Another way to determine the distrust level is to rigidly set it to 0 or 1. In our previous study [5], we used such a distrust level in determining the authenticity of rescue requests in the event of flooding. This case concerns the determination of the distrust level in unusual circumstances.

During the torrential rainstorm in western Japan in 2018, many rescue requests were posted on SNS, and detailed address information on the posters appeared in some of those messages. Personal addresses are typically private information, and people regularly do not post them unnecessarily on SNS. Posting a private address indicates that the poster was really in imminent danger. Hence, the credibility of such a message as a rescue request becomes high.

[4]In this footnote, we provide a more detailed analysis for the pairs of (i_c, c_c). For country X, there is some degree of distrust of the government, and citizens in country X are somewhat confused since the degree of contradiction is positive. For country Y, the degree of trust exceeds the degree of distrust, but the degree of contradiction is negative, which suggests that the people have little interest in their government. For countries Y and Z, although their integration values are the same, the degree of contradiction is positive for country Z. Note that we can compare countries Y and Z, even though the conventional trust model cannot since the degree of contradiction is not addressed.

- I am the person who called for rescue after the heavy rain in Arii, Mabi-cho, Kurashiki City. I have just been rescued safely. Thank you very much for your concern. I will delete this tweet to avoid confusion. Thank you for your cooperation. #Kurashiki #Mabi-cho
- #Rescue completed #Kurashiki-shi, Mabi-cho, Arii XXX. We have received a report that they have been rescued safely. Sorry for your concern. Thank you so much.

Figure 6: Non-rescue requests containing (nearly) complete address information

However, in an emergency, when determining whether a message is a genuine rescue request, it is natural that the distrust level reaches maximum if there is even one suspicious element. Note that this approach to determining the distrust level differs from the cumulative approach used in the previous section.

Figure 6 shows some postings in the above disaster. In these messages, words such as "thank you" or "sorry for your concern" appear disproportionate to a rescue request. Therefore, the distrust level is set to 1, resulting in a low one-dimensional trust value. Such phrases typically appear in messages that report the completion of the rescue, citing past actual rescue requests.

For the application to job search assistance shown in this paper, we also set the distrust level to 0 or 1, considering students tend to avoid firms with "undesired items" because it may affect their later life. Summarizing, we can see the following:

- For the case of judging rescue requests in the event of flooding, we should employ a high distrust level to exclude information that would interfere with rescue because human lives are at stake; and
- For the case of job search assistance, students want to use a high distrust level since they wish to exclude any job information containing undesired conditions.

From this observation, we use the distrust levels at extremities (i.e., near 0 or 1) to vehemently reject information that is not appropriate for related parties, as in the case of the two examples listed in this section. In other words, this type of distrust determination method should be used when the impact of the failure is significant for the parties concerned. A detailed examination of the validity of this approach is a future issue.

5 DISCUSSIONS

In this study, trust values were obtained and used based on the company profiles' location and job type information. We have a further discussion on the application of this trust value in this section.

Although this study mainly focuses on preferences for work location and job type, some may question the influence of

other priorities, such as salary and company size. Although location and job type are not everything in job hunting, we chose these criteria in this case study because, in our experience, the target students tend to place importance on "location" and "job type." In reality, students decide which company to work for by considering other information, such as their impression of the company when they visit the company. We believe that it is possible to calculate the degrees of trust and distrust for other preference items.

This study independently treats the two types of preferences, i.e., work location and job type. In general, it isn't easy to automatically handle the interdependence of multiple preferences, and this paper's case study did not treat it. Consider the following example, in which the conditions for the location and job preferences are contradictory.

Example 2 *Please assume that the student's favorite place is Nagoya, his disliked place in Hokkaido, and his favorite job is software development. Also, please assume that the company has its headquarters in Nagoya and a software development center in Hokkaido.*

In this study, location preference and job type preference are treated independently. For this company, a location that the user dislikes (Hokkaido, Japan) is included in the job posting, and a high level of distrust is assigned to the site, so the company is either excluded from the list of companies to be presented, or presented at the end of the list. However, the final decision based on multiple preferences is made by the user, the student. One student may prioritize location preference, while another may be more concerned about the type of job. Since there may be other criteria, we believe that it is difficult to make this decision automatically. Therefore, this study treated the evaluation results (i.e., one-dimensional trust values) for work location and job type independently and presented them together.

A one-dimensional trust value based on trustworthiness alone may not compare the trust values of job postings from two companies, or it may result in a company that the student does not want to remain on the list of companies. We consider the following example.

Example 3 *Assume that the student showed three favorite places. Also, assume that a company showed just the same three places. Another company showed ten sites, including the three places.*

In this example, since the same values are computed for the positive part of trustworthiness, the job postings are incomparable only when dealing with the positive trust levels. However, when we consider the distrust levels, the corresponding one-dimensional trust of the locations of these companies may have different values. If the second firm has an undesired location among the seven remaining sites, the one-dimensional trust value will be lower[5]. Since this study treats distrust independently, comparing two firms that do not differ only in this evaluation of trustworthiness is possible.

[5]Suppose the remaining seven workplaces do not include the unwanted workplaces. In that case, the student can either ignore the seven workplaces as "workplaces that the student does not refuse," or he can re-enter the unwanted workplaces and re-create the list again using the tool in this study.

While this study delves into the intricate realm of evaluating corporate information using two-dimensional trust values, some readers may be tempted to compare these findings with the more conventional method proposed by Marsh et al. In reality, however, it is not easy to do so. Our previous study [4] showed that Marsh et al.'s one-dimensional trust values correspond to the case where we allow a strong restriction: "The sum of trustworthiness and distrustworthiness is exactly one in a two-dimensional trust representation." This result means that when we make the same evaluation as in the present experiment using 1D trust values, we should assume that students have in their minds 1D trust values that satisfy the condition of the definite sum; for example, the trust value of a company's job information is 0.76, and the distrust value is 0.24, and these values can be correctly quantified. However, making such an assumption is difficult, at least in applications like the one treated in this study. In this study, we do not assume such a sum scale but allow for ambiguity regarding people's level of trust in and distrust of the target. By obtaining "trustworthiness" and "distrustworthiness" for each of the items of work location and job type from "degree of conformity with expectations" and "presence or absence of unwanted items," respectively, it can be said that this study approximates "the true trust value in the minds of students" regarding corporate information. Although these approximated values do not always satisfy the conditions of the definite sum, by calculating the integrated value, "the evaluation value based on the two-dimensional trust theory is translated into the evaluation value of the one-dimensional trust theory." As a result, the evaluation value of the definite sum scale, which is difficult for people to answer directly, is objectively obtained.

In addition to this, the question of whether it is appropriate to treat students' occupational preferences with a trust concept may also arise. In this study, the observer is a student, and the trustee is job information; note that in the trust theory, the trustee is not necessarily a person. Following the definition of the trust concept in section 2.1, the trust value (after being converted to a one-dimensional value) holds a pivotal role. It corresponds to the degree to which the student believes the job information. When the trust value is sufficiently high, it fosters a strong belief in the students, leading to a positive perception of the job information. When the one-dimensional trust value is negative, the student believes some of the job information may work against the student in the job-hunting situation. Actually, including unacceptable information may work against the student. Furthermore, when the evaluation result shows an "untrusted" case, the evaluator cannot determine whether the job information is trustworthy enough to adopt. In summary, the trust value represents "whether the given job information is desirable to the student." Therefore, evaluating students' job preferences using trust theory is appropriate, and we can see that it is a good application.

6 CONCLUSION

This study treated the job-matching problem as a practical application of the two-dimensional trust model. The definition of the two-dimensional trust value presented in our previ-

ous study (or Section 2) described how to determine the range of trust/distrust values and calculate the integration value, which corresponds to Marsh et al.'s one-dimensional trust value. However, it did not specify how to determine the values of trust and distrust levels in specific cases. Therefore, this paper has presented the job-matching problem as a concrete example of using these values, especially for applying distrust in an emergency. We also have shown how to determine the distrust level in the job matching problem. We assigned 0 or 1 instead of any value between 0 and 1 to reject information that is not appropriate for the student vehemently. Furthermore, we discussed how to determine the distrust level in two possible cases (cumulative distrust level and non-cumultive distrust level), paying particular attention to the similarities with the case of message classification in the event of flooding. A two-dimensional trust that considers the distrust level can be used to compare two companies that cannot be compared only based on trustworthiness or to eliminate inappropriate information using the distrust level.

We developed a recommender system for students' job-finding assistance. After collecting information on job openings and student preferences, we calculated the two-dimensional trust values that represent the fitness of matching between the student and the company. However, the two-dimensional trust value may be inconsistent since the trust and distrust parts are given independently. This study obtained a corresponding one-dimensional trust value for a consistent evaluation; specifically, we got the one-dimensional trust value by calculating the integration value of Oda's FCR method. Then, we employed the resulting trust value in the recommendation process. In this study, we also discussed determining the distrust levels.

This paper uses a coarse criterion that we only use, either 0 or 1, to determine the distrust level. As indicated in this paper, there are cases where this idea is sufficient as a criterion of distrust. However, under this criterion, although it is possible to "reject" messages containing inappropriate information, it is difficult to "finely discount" the messages' trust level. Hence, introducing a finer (i.e., not too coarse) evaluation of distrust levels as future work is essential. A trust concept called swift trust [12, 13] is necessary for building cooperative relationships between victims and volunteers during a large-scale disaster [14–16]. We believe the idea of not-too-coarse distrust levels helps evaluate the swift trust. It is also necessary to provide criteria for which type of distrust we should employ in which situations. It is also an interesting issue.

ACKNOWLEDGMENT

This study is partly supported by the Grant-in-Aid for Scientific Research (C), No. 24K14957, of the Ministry of Education, Culture, Sports, Science and Technology, Japan.

REFERENCES

[1] T. Oda, "Measurement technique for ergonomics, section 3: Psychological measurements and analyses (3) measurements and analyses by kansei evaluation," *The Japanese Journal of Ergonomics*, vol. 51, no. 5, pp. 293–303 (2015). In Japanese.

[2] J. Deng, T. Oda, and M. Umano, "Fuzzy logical operations in the two-dimensional hyper logic space concerning the fuzzy-set concurrent rating method," *Journal of Japan Association for Management Systems*, vol. 17, no. 2, pp. 33–42 (2001).

[3] K. Ohkubo, T. Oda, Y. Koizumi, T. Ohki, M. Nishigaki, T. Hasegawa, and Y. Kawabe, "Trust representation under confusion and ignorance," in *Proceedings of International Workshop on Informatics (IWIN 2018)*, pp. 191–198 (2018).

[4] Y. Kawabe, Y. Koizumi, T. Ohki, M. Nishigaki, T. Hasegawa, and T. Oda, "On trust confusional, trust ignorant, and trust transitions," in *Trust Management XIII - 13th IFIP WG 11.11 International Conference, IFIPTM 2019, Copenhagen, Denmark, July 17-19, 2019, Proceedings*, pp. 178–195 (2019).

[5] Y. Kawabe, Y. Koizumi, T. Ohki, M. Nishigaki, and T. Hasegawa, "Finding trustable rescue requests with Zip numbers," in *The 37th Fuzzy System Symposium (FSS 2021)*, pp. 601–606 (2021). In Japanese.

[6] S. Marsh and M. R. Dibben, "Trust, untrust, distrust and mistrust – an exploration of the dark(er) side," in *Proceedings of the Third International Conference on Trust Management*, iTrust'05, (Berlin, Heidelberg), pp. 17–33, Springer-Verlag (2005).

[7] G. Primiero, "A calculus for distrust and mistrust," in *Trust Management X* (S. M. Habib, J. Vassileva, S. Mauw, and M. Mühlhäuser, eds.), (Cham), pp. 183–190, Springer International Publishing (2016).

[8] G. Primiero, F. Raimondi, M. Bottone, and J. Tagliabue, "Trust and distrust in contradictory information transmission," *Applied Network Science*, vol. 2, p. 12 (2017).

[9] R. J. Lewicki, D. J. B. McAllister, and R. J. Bies, "Trust and distrust: New relationships and realities," *Academy of Management Review*, vol. 23, pp. 438–458 (1998).

[10] A. Jøsang, *Subjective Logic: A Formalism for Reasoning Under Uncertainty*. Springer Publishing Company, Incorporated, 1st ed. (2016).

[11] "MeCab: Yet another part-of-speech and morphological analyzer." `https://taku910.github.io/mecab/`, (accessed October 4, 2024).

[12] D. Meyerson, K. E. Weick, and R. M. Kramer, *Swift Trust and Temporary Groups in Trust in Organizations: Frontiers of Theory and Research*. SAGE (1995).

[13] J. Wildman, M. Shuffler, E. Lazzara, S. Fiore, and S. Burke, "Trust development in swift starting action teams: A multilevel framework," *Group & organization management*, vol. 37, no. 2, pp. 137–170 (2012).

[14] M. G. Busa, M. T. Musacchio, S. Finan, and C. Fennell, "Trust-building through social media communications in disaster management," in *Proceedings of the 24th International Conference on World Wide Web*, WWW '15 Companion, (New York, NY, USA), pp. 1179–1184, ACM (2015).

[15] F. Lemieux, "The impact of a natural disaster on altruistic behaviour and crime," *Disasters*, vol. 38, pp. 483–

499 (2014).
[16] Y. Murayama, “Issues in disaster communications,” *Journal of Information Processing*, vol. 22, no. 4, pp. 558–565 (2014).

(Received: November 15, 2023)
(Accepted: September 5, 2024)

Yoshinobu Kawabe received his B.E., M.E., and D.E. degrees in information engineering from Nagoya Institute of Technology in 1995, 1997, and 2003. He joined NTT Communication Science Laboratories, Nippon Telegraph and Telephone Corporation in 1997. In 2002, he was a visiting research scientist at MIT Laboratory for Computer Science. Since 2008, he has been at Aichi Institute of Technology, where he is a professor at the Department of Information Science. His research interests include term rewriting systems, process algebras, network programming languages, formal methods, security/privacy verification, and computational trust. He is a member of ACM, JSSST, IPSJ, SOFT, and IEICE.

Tetsuhisa Oda received a B.E. degree from Tokyo University of Science in 1971. He also received M.E. and PhD degrees from Waseda University in 1976 and 2002, respectively. He served as a professor at Aichi Institute of Technology until 2018 and is currently a professor emeritus. His main research area is the application of fuzzy logic to psychology. He is a member of the Japanese Society for Fuzzy Theory and Intelligent Informatics, the Japan Association for Management Systems, president from 2015 through 2017, the Japanese Psychological Association, and the Operations Research Society of Japan.

Regular Paper

Autonomous Driving on Community Roads Using Small Mobility: Route Generation Using Trajectory Prediction and 2D TTC

Takumi Seita*, Shunsuke Michita*, Seiji Komiya*, and Toshihiro Wakita*

*Graduate School of Engineering, Kanagawa Institute of Technology, Japan
s2384004@cco.kanagawa-it.ac.jp

Abstract - Traffic accidents occur frequently on community roads where pedestrians and vehicles coexist, therefore safe and smooth autonomous driving is expected. Based on this situation, this paper proposes a path planning method for autonomous vehicles by extending the Velocity Obstacles algorithm (VO). VO is commonly used in mobile robotics. Three points were extended to apply the algorithm. The first point was to use 2D TTC to reduce unnecessary avoidance. It was decided that avoidance would not be performed if there is room for it based on the 2D TTC calculation of collision time. The second point established motion constraints by assuming avoidance is performed with steady-state circular motion because vehicles have more motion constraints than robots. The third point was to change the collision detection method from circle approximation. Considering the size and shape of the vehicle, it was decided to draw tangents from the four corners of the vehicle to the obstacle and combine them. Using the above algorithm, avoidance paths were generated and better performance than VO, DWA and risk potential method.

Keywords: Autonomous Mobility, Pedestrian prediction

1 INTRODUCTION

1.1 Background

In recent years, although the reduction of traffic accident fatalities has been decreasing, the decreasing trend of the number of traffic accidents on community roads has remained relatively low. According to data from the Ministry of Land, Infrastructure, Transport and Tourism, in 2021, there were approximately 80,000 traffic accidents on community roads, compared to approximately 220,000 accidents on arterial roads [1]. In terms of the reduction rate since 2004, arterial road accidents have decreased by about 70%, while community road accidents have decreased by about 60%. Therefore, in order to reduce traffic accidents on community roads as well as arterial roads, the realization of safe and efficient autonomous driving is desired.

However, community roads have distinct characteristics such as the lack of white lanes, pedestrians freely walking along various paths, and narrow road widths, making a significantly different traffic environment compared to arterial roads. Because there are numerous problems that differ from previous autonomous driving environment, it difficult to achieve autonomous driving on community roads.

1.2 Related Research

Autonomous navigation in complex environments like community roads has been extensively studied in the context of mobile robots. Various research has been conducted on obstacle avoidance methods for mobile robots.

The dynamic window approach (DWA) [2] is an approach that generates trajectory candidates by combining translational and rotational velocities. It evaluates each generated trajectory using an evaluation function. Following that, the trajectory with the highest evaluation value is selected, and the robot follows that trajectory. One of the problems of this method is that it does not consider dynamic obstacles, which may result in insufficient avoidance of dynamic obstacles such as pedestrians.

The risk potential method [3] defines repulsive potentials and an attractive potential to the target reaching position to obstacles. It generates target velocities and target paths based on the calculated potential gradients. One of the problems of this method is that the generated potential field is a virtual quantity without physical meaning. Due to the lack of physical significance, parameter adjustments are required, making it difficult to achieve proper control of the trajectory, velocity, and adaptation to various traffic environments.

The freezing robot problem (FRP) have focused on predicting the future actions of pedestrians using Social LSTM [4] and avoiding areas that may obstruct pedestrians (Potential Freezing Zone: PFZ) [5]. However, these methods address only pedestrians.

There is a VO algorithm [6] as a method to avoid various dynamic obstacles such as pedestrians, bicycles, and other vehicles. VO is a method for motion planning of a robot in a dynamic environment with moving obstacles. This method defines a "velocity obstacle" as the velocity space within which a robot may have potential collisions based on the current positions and velocities of the robot and obstacles. By calculating velocity obstacles for all obstacles and selecting a velocity that does not belong to any velocity obstacle, this method generates obstacle-avoiding trajectories. VO is considered suitable for path planning on community roads, as it is an effective method for avoiding dynamic obstacles.

Up to now, various extensions have been attempted in VO. Reciprocal Velocity Obstacles (RVO) [7] address the vibration problems that arise when VO robots need to avoid each other. Optimal Reciprocal Collision Avoidance (ORCA) [8] addresses the shortcomings of RVO, which only guarantees collision avoidance under specific conditions and does not provide a sufficient condition for general collision avoidance. This method presents sufficient conditions for multiple robots to avoid collisions with each other, ensuring collision-free navigation. Adaptive Velocity Obstacles (AVO) [9] is proposed to solve that if the robot chooses the critical velocity of the collision cone to minimize the time consumption, the error of the sensor will lead to the collision. Ellipse-based Velocity Obstacles (EBVO) [10] derived the VO for an elliptic robot, and showed that the robot could reach the goal with a less traveled path by controlling the rotary motion. As these extensions are not effective for path planning on community roads where it is necessary to avoid obstacles such as pedestrians and other vehicles, this study attempted to apply the original VO algorithm.

1.3 Research Question

VO is suited for mixed pedestrian and vehicular environments on community roads, but it originally developed for mobile robots. Consequently, adapting VO directly to vehicles in mixed pedestrian and vehicular environments on community roads appears several problems.

The first problem is the existence of numerous pedestrians. On community roads, there are often many pedestrians walking in various directions along narrow roadways. When applying VO to such situations, the velocity space may become entirely covered by velocity obstacle regions, leaving no viable velocity options.

The second problem is related to achieving the selected velocity. In VO, the velocity pair v_x , v_y that can reach the goal fastest among velocities not belonging to the velocity obstacle region is chosen. Many mobile robots are equipped with differential drives or omnidirectional wheels, making it relatively easy to achieve the selected velocity. However, in case of automobiles, which mostly adopt front-wheel steering and have longer wheelbases, there are significant constraints on achievable velocities. As a result, there can be a significant difference between the selected velocity and the realized velocity, potentially leading to inappropriate trajectory generation.

The third problem relates to road width. Generally, community roads have narrow roadways, which limits the freedom of path selection. On the other hand, in VO, there are cases where a viable velocity is not selected despite being capable of driving on narrow roads. One reason is that VO approximates both pedestrians and the ego vehicle with circles for collision detection. Since the shape of automobiles often differs significantly in terms of width and length, there can be a significant difference between the actual collision detection and the circle approximation. Additionally, the circular approximation tends to generate avoidance paths that take unnecessarily large avoidance distances from obstacles. As a result, on narrow community roads, there can be situations where no velocity candidates are available.

To address these problems, this study attempts to achieve autonomous driving on community roads by extending the capabilities of VO. The extended method is referred to as VO-drive in this research.

2 METHODS

2.1 VO

VO is a method for motion planning of a robot in a dynamic environment with multiple moving obstacles. In this algorithm, based on the current positions and velocities of the robot and obstacles, the velocity space of the robot that may lead to future collisions is defined as the "velocity obstacle." The positions of the robot and obstacle are presented as **A** and **B**, respectively, and their velocities as $\mathbf{v_A}$ and $\mathbf{v_B}$. The size of the robot and obstacles are approximated by circles circumscribing them. Each radius is presented R_A and R_B , respectively. The circle centered at **B** with a radius of $R_A + R_B$ is defined as the collision circle. In this case, the set of relative velocities $\mathbf{v_{A,B}}$ that would result in a collision between **A** and **B** forms a collision cone $\boldsymbol{CC_{A,B}}$ (Fig. 1).
The collision cone $\boldsymbol{CC_{A,B}}$ is a planar region bounded by two tangents, λ_f and λ_r, from **A** to the collision circle. In this region, the relative velocity $\mathbf{v_{A,B}}$ between the robot and the obstacle would result in a collision. Thus, the region of relative velocities $\mathbf{v_{A,B}}$ that lead to a collision is determined.

Next, the region of robot velocities $\mathbf{v_A}$ that would result in a collision is calculated. The obstacle velocity $\mathbf{v_B}$ is added to each velocity in the collision cone $\boldsymbol{CC_{A,B}}$. This is equivalent to translating $\boldsymbol{CC_{A,B}}$ by the velocity $\mathbf{v_B}$ (Fig. 2). If the robot velocity $\mathbf{v_A}$ lies within this translated collision cone, a collision would occur. Therefore, this translated collision cone is referred as the "velocity obstacle."

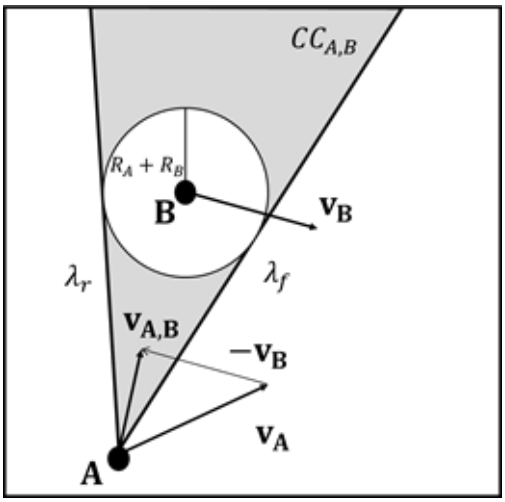

Figure 1 Relative distance $\mathbf{v_{A,B}}$ and collision cone $\boldsymbol{CC_{A,B}}$

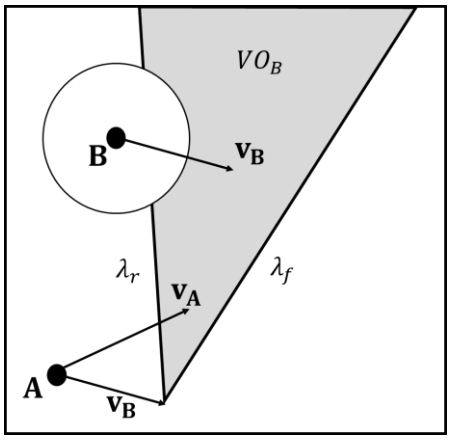

Figure 2 velocity obstacle

The selection of velocity for robot motion is performed as follows. First, an initial velocity is calculated based on a predetermined magnitude of velocity, assuming no obstacles. If the initial velocity lies outside the velocity obstacle, it is directly used for motion. If the initial velocity lies within the velocity obstacle, the velocity closest to the initial velocity on the outside of the velocity obstacle is selected and used for motion.

2.2 VO-Drive

To adapt VO to community roads and autonomous driving, three extensions were made.

2.2.1 Limitation of the Target Object

The first extension addresses the issue of handling a large number of pedestrians. In community roads, there may be many pedestrians walking in various directions along narrow roadways. When applying VO to such a situation, the velocity space is covered by the velocity obstacle region, and no available velocities become exist. To resolve this, a method can be considered to limit the pedestrians (obstacles) that need to be avoided using some criteria. Possible criteria include distance, direction, etc. In this study, a two-Dimensional Time To Collision (2D TTC) based on the time margin until collision is used [11]. It is known that 2D TTC is related to pedestrians' sense of safety in collision avoidance for mobile robots. Therefore, pedestrians with a 2D TTC value above a certain threshold can be considered to have a lower risk of collision and can be excluded from collision detection.

Time To Collision (TTC) is a physical indicator used in Autonomous Emergency Braking (AEB) systems in vehicles. This indicator represents the time until collision with a leading vehicle if the current relative velocity between the ego vehicle and the leading vehicle is maintained. In the world coordinate system, the ego vehicle's front-end position and velocity are presented as x_e and v_e, respectively, while the leading vehicle's rear-end position and velocity are presented as x_l and v_l, respectively. In this case, the relative distance, d_x, and relative velocity, v_x, between the host vehicle and the leading vehicle can be calculated as $x_l - x_e$ and $v_l - v_e$, respectively (Fig. 3).

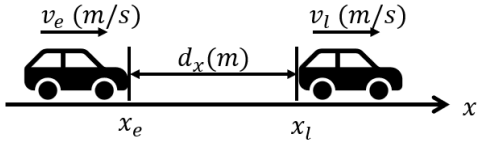

Figure 3 TTC outline figure

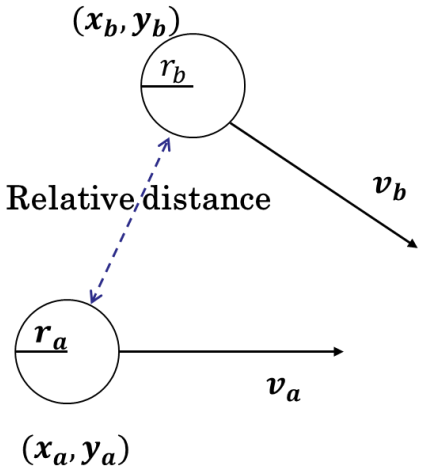

Figure 4 2D TTC outline figure

Therefore, the value of TTC, presented as t_x, can be expressed by the following equation (1).

$$t_x = -\frac{d_x}{v_x} = -\frac{x_l - x_e}{v_l - v_e} \tag{1}$$

In this study, the 2D extension of TTC, referred to as 2D TTC was used. This index takes into account the positional relationship in a 2D space considering the vehicle's longitudinal direction (x-axis in the vehicle coordinate system) and lateral direction (y-axis in the vehicle coordinate system), whereas the previous TTC was calculated based on the positional relationship along the vehicle's longitudinal direction (x-axis) only. In the world coordinate system, the position of the ego vehicle is represented as (x_a, y_a), the position of the obstacle is represented as (x_b, y_b), the velocity of the ego vehicle is presented as (v_{ax}, v_{ay}), the velocity of the obstacle is presented as (v_{bx}, v_{by}), the size of the ego vehicle is presented as r_a, and the size of the obstacle is presented as r_b. Therefore, the relative distance is calculated as $\sqrt{(x_b - x_a)^2 + (y_b - y_a)^2}$, and the relative velocity is calculated as $\sqrt{(v_{bx} - v_{ax})^2 + \left(v_{by} - v_{ay}\right)^2}$ (Fig. 4). Therefore, the value of the 2D TTC is given by the following equation (2).

$$TTC_{2d} = \frac{\sqrt{(x_b - x_a)^2 + (y_b - y_a)^2} - (r_a + r_b)}{\sqrt{(v_{bx} - v_{ax})^2 + \left(v_{by} - v_{ay}\right)^2}} \tag{2}$$

Pedestrians with a 2D TTC value equal to or greater than a certain threshold are considered not requiring avoidance and are therefore excluded from the velocity obstacle calculations.

2.2.2 Velocity Selection Based on Vehicle Motion Constraints

The second point is addressing vehicle motion constraints. Unlike mobile robots, automobiles have significant motion constraints, so an extension was made to select velocities achievable by car steering.

First, assuming the vehicle is either moving straight or performing a steady-state circular motion, the trajectory is calculated [12]. The illustration of this is shown in the figure below (Fig. 5). Let θ be the angle between the X-axis and the vehicle's longitudinal direction (yaw angle), β be the angle between the vehicle's direction of travel and its longitudinal direction (slip angle), r be the angle between the X-axis and the vehicle's direction of travel, and V be the vehicle's velocity. The slip angle is determined by Equation (3), and the angle between the X-axis and the vehicle's direction of travel is given by Equation (4).

$$\beta = \left(\frac{1-\frac{m}{2l}\frac{l_f}{l_r K_r}V^2}{1-\frac{m}{2l^2}\frac{l_f K_f l_r K_r}{K_f K_r}V^2}\right)\frac{l_r}{l}\delta \tag{3}$$

$$r = \left(\frac{1}{1-\frac{m}{2l^2}\frac{l_f K_f - l_r K_r}{K_f K_r}V^2}\right)\frac{V}{l}\delta \tag{4}$$

Therefore, the trajectory of the moving vehicle's center of gravity is considered. The positions and velocities of the vehicle and the obstacle in the world coordinate system are shown in the figure below (Fig. 6). Let (x_e, y_e) and (v_{ex}, v_{ey}) represent the position and velocity of the vehicle, respectively, and (x_p, y_p) and (v_{px}, v_{py}) represent the position and velocity of the obstacle. The obstacle is assumed to move in a straight line at a constant speed, and its trajectory is predicted.

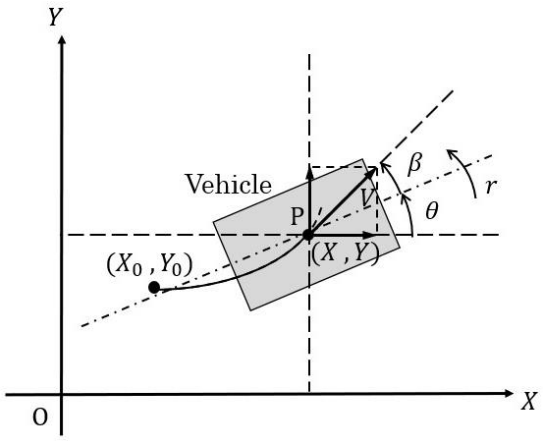

Figure 5 Vehicle trajectory prediction

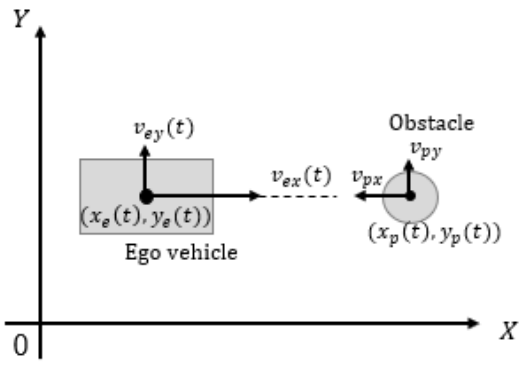

Figure 6 Each variable in the world coordinate system

Given the initial position (X_0, Y_0) and the initial yaw angle θ_0, the position (X, Y) and the yaw angle θ at any given time t can be calculated using equations (5), (6), and (7).

$$X = X_0 + V\int_0^t \cos(\beta+\theta)\,dt \tag{5}$$

$$Y = Y_0 + V\int_0^t \sin(\beta+\theta)\,dt \tag{6}$$

$$\theta = \theta_0 + \int_0^t r dt \tag{7}$$

The actual calculation process is outlined below.

Step1 Provide steering angle for ego vehicle.

Step2 Calculate β and r using the steering angle from Step1 according to equations (3) and (4).

Step3 Using equations (5) and (6) from Step2, calculate the reachable points.

Step4 Calculate the velocity required to reach the speed in Step3.

Step5 Convert the velocity in Step4 to the velocity within the VOmap.

Step6 Prepare a map similar to VOmap, and substitute the value of the steering angle at the velocity position in Step5.

Step7 Repeat Step 1 to 6.

Here is the outline of trajectory prediction (Fig. 7).

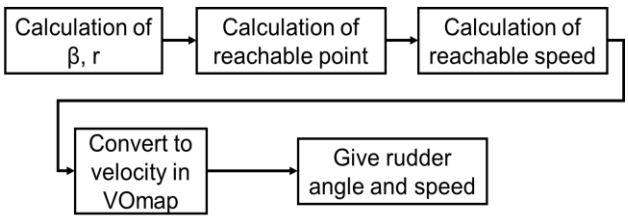

Figure 7 Outline of trajectory prediction

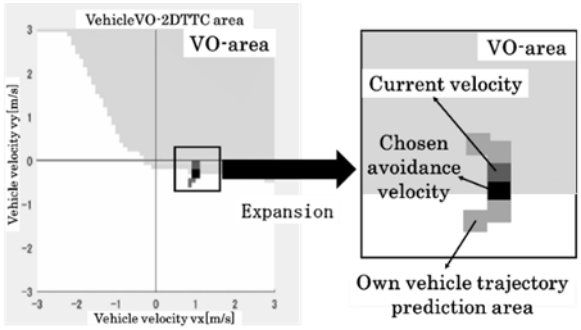

Figure 8 Example of trajectory prediction

However, there is a difference when combining the VO method with trajectory prediction. VO assumes both the ego vehicle and the obstacles move in constant linear motion and generate avoidance paths based on the assumption that the current velocity will continue. On the other hand, trajectory prediction for constant circular motion involves nonlinear motion with constant translational and rotational velocities, making it incompatible to directly apply the VO method.

Therefore, in this case, an attainment point based on the current velocity that would result in a constant circular motion was assumed. The line connecting the starting point and the attainment point was approximated.

The generated trajectory prediction points for the ego vehicle are shown in the figure below (Fig. 8).

2.2.3 Collision Detection Based on the Vehicle Contour

The third point addresses the issue of narrow road widths. In the VO approach, both pedestrians and ego vehicles are approximated as circles for collision detection. However, this approximation can result in significant differences between the actual collision detection and the circle approximation. Using circular approximation often leads to unnecessarily large avoidance routes.

According to the Japanese Cabinet Office, a "community road width" is defined as a road with a carriageway width of less than 5.5 meters in urban areas. If the avoidance route is too large, there is a risk of veering off the road or even the possibility of being unable to avoid the obstacle altogether. To achieve a compact and safe avoidance route, a collision detection method that takes into account the vehicle's contour was adopted (Fig. 9).

By utilizing the vehicle's contour, performing VO calculations from the four corners of the vehicle to the obstacles. Figure 10 shows velocity obstacle area. The original VO area is shown in gray and extended method area shown in black. This shows that it can be observed that extended method results in a smaller area compared to the original method. This approach allows for more precise collision detection and avoidance planning, taking into account the actual shape and size of the vehicle.

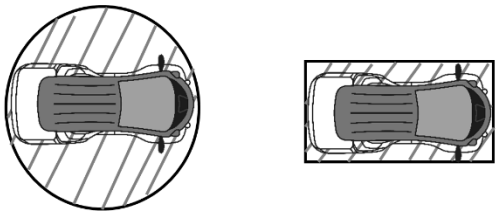

Figure 9 Comparison between circle approximation and contour-based methods

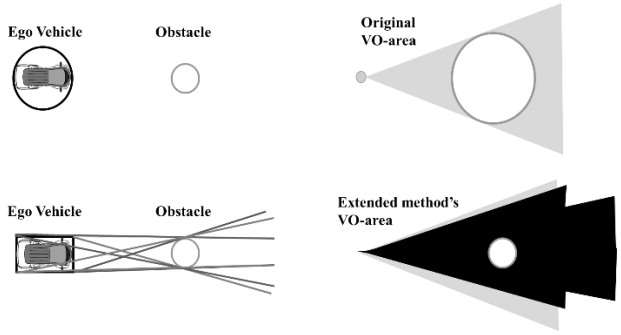

Figure 10 Caomparison of calculation methods between original VO and extended method

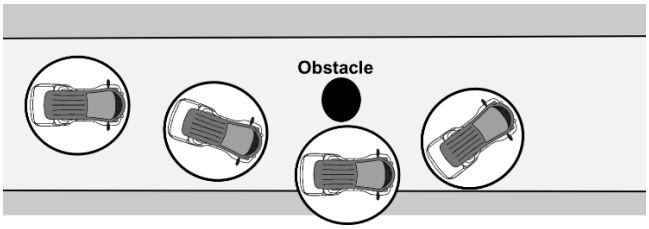

Figure 11 Example of avoidance using circle approximation

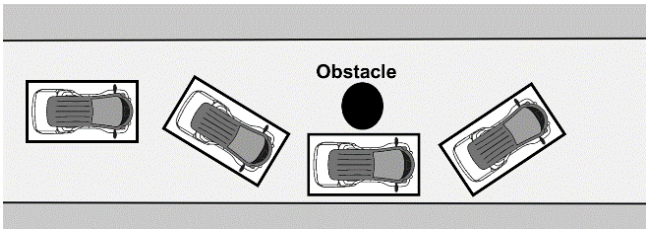

Figure 12 Example of avoidance using vehicle contour

When actually performing circular approximation in a scenario simulating a community road environment, as shown in Fig. 11, attempting to avoid obstacles leads to deviating from the lane due to the constraints of the road width. Therefore, by performing calculations from the four corners of the vehicle, it becomes possible to avoid obstacles while staying within the lane width, as shown in Fig. 12. This approach ensures that the vehicle navigates safely within the available space and minimizes the risk of deviating off the road.

3 SIMULATION EXPERIMENT AND RESULTS

3.1 Experimental Conditions

Using the VO-drive method proposed in this study, a simulation experiment was conducted to compare it with the original VO (Velocity Obstacle) method, DWA (Dynamic Window Approach), and the risk potential method.

The simulation was performed using MATLAB. A time step of 0.1 seconds was used, and the initial value of the vehicle speed was set to 15 km/h. When the path generation method instructed a specific speed, it followed the generated speed by each route generation accordingly.

About the risk potential method, only the repulsive potential from obstacles was defined [13]. The repulsive potential was calculated by the distance from the surface of obstacle. Here, $P_{repulsive}$ shows repulsive potential energy, K_{rep} shows repulsion coefficient, and $distance_{ob}$ shows distance to the obstacle. The expression for the repulsive potential energy is given as Equation 8.

$$P_{repulsive} = \sum \left(\frac{K_{rep}}{distance_{ob}} \right) \tag{8}$$

When TTC falls below 6 seconds, the route is generated to select areas with lowest potential.

DWA (Dynamic Window Approach) requires the setting of three weights: goal direction weight, obstacle distance weight, and velocity weight. In this experiment, these weights were set to 0.1, 0.2, and 0.3, respectively.

For VO-drive, the threshold for 2D TTC was set to 6 seconds as a limitation condition for the target obstacle. Only obstacles with TTC values below this threshold are considered for avoidance. And, the attainment point was defined as the point reachable 0.1 seconds later. For obstacle behavior prediction, the walking speed of the tracked obstacle was calculated using a Kalman filter, and the predicted position was calculated based on the calculated walking speed [14].

3.2 Comparison Between VO-Drive and VO

First, a comparison was conducted between the original VO and the extended VO-drive to confirm the effectiveness of the extension.

A comparative experiment was conducted on the limitation of the target obstacle. The results are shown in Fig. 13. The ego vehicle starts from the position (-15,0) in the world coordinate system and moves straight at a speed of 15 km/h. An experimental scenario was designed where the vehicle needs to avoid a stationary obstacle located at (15,0). From Fig. 13, it can be observed that the extended VO-drive leads to a delay in the timing of avoidance initiation. Conventional VO begins avoidance from the start point, whereas the extended VO-drive proceeds straight initially due to the absence of collision risk and begins avoidance only upon detecting a potential collision danger.

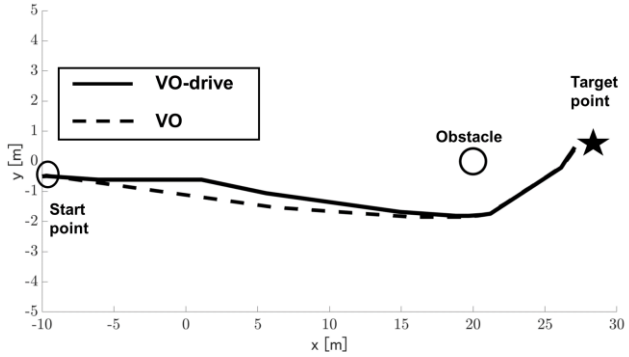

Figure 13 Comparison of target obstacle limitation

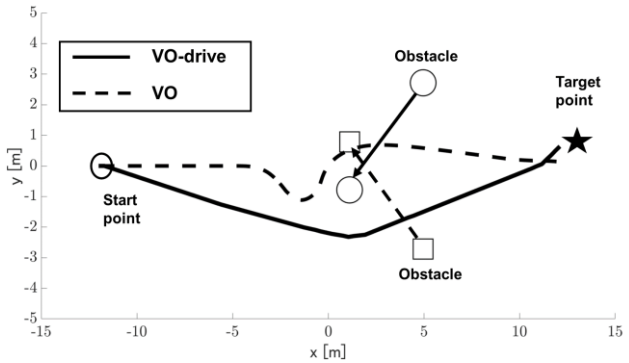

Figure 14 Comparison of vehicle motion constraints

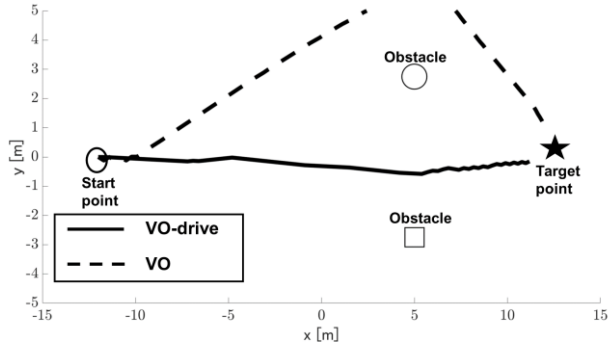

Figure 15 Comparison of collision detection

Second, a comparative experiment was conducted on velocity selection based on vehicle motion constraints. The results are shown in Fig. 14. The ego vehicle starts from the position (-12,0) in the world coordinate system and moves straight at a speed of 15 km/h. Two obstacles are introduced, each moving diagonally at a speed of 0.5 m/s, creating a crossing scenario. From Fig. 14, it can be observed that the proposed method achieves smoother and more efficient avoidance, while the original VO approach exhibits sharp turns.

Lastly, a comparative experiment was then conducted on collision detection based on the vehicle contour. The results are shown in Fig. 15. The ego vehicle starts from the position (-12,0) in the world coordinate system and moves straight at a speed of 15 km/h, aiming to compare whether it can navigate between the obstacles. From Fig. 15, it can be observed that the conventional circle approximation method fails to navigate between the obstacles and takes a significantly larger avoidance path, while the extension allows the vehicle to pass between the obstacles successfully.

3.3 Comparison of VO-Drive and Other Methods

Then, a comparison was made between the proposed VO-drive method and the original VO, DWA, and risk potential method. The horizontal lines shown in the figure represent the width of the community roads, with the width between the upper and lower lines being 5.5m. The experiment scenario was the same as described earlier, with two diagonal-crossing obstacles. In the figures, the distance traveled by each method is shown at the same elapsed time as the progress of the VO-drive method. The elapsed time in the experiment was 23 seconds. The results are shown in Fig. 16. From Fig. 16, it can be observed that the VO-drive method has traveled the farthest within the same elapsed time. The original VO method exhibits similar behavior as in Fig. 14. DWA shows larger avoidance routes compared to the VO-drive method. The risk potential method failed to avoid and came to a stop.

The final generated trajectories are shown in Fig. 17. The elapsed time and maximum avoidance amount for each method until reaching the target point are shown in Table 1. It is evident that the proposed method, VO-drive, achieves the shortest time and maintains avoidance within the road width. VO achieves avoidance with some margin to the road width but takes longer to avoid. DWA avoids by a larger margin than the road width. Regarding the risk potential method, it failed to avoid the obstacle, resulting in a collision after 17 seconds.

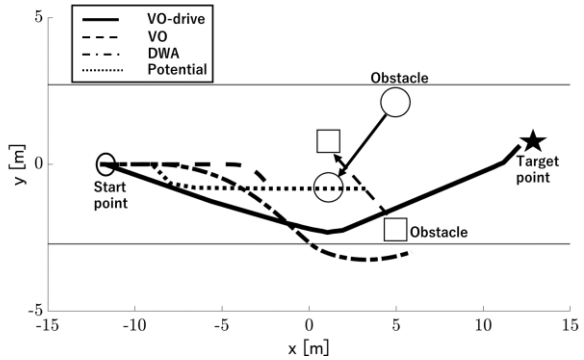

Figure 16 Trajectories of each method at 23 seconds elapsed

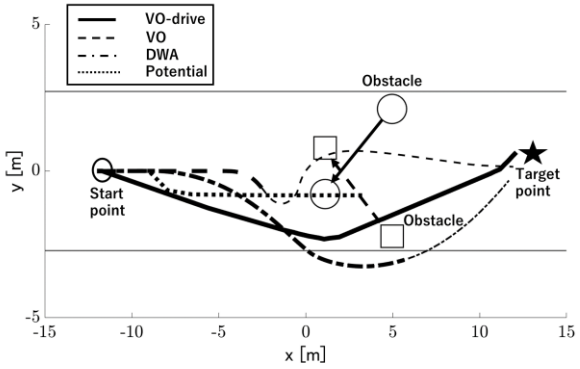

Figure 17 The generated trajectories in the end

Table 1 Comparison of results for each method

	The elapsed time (s)	The maximum avoidance amount (m)
VO-drive	23	2.32
VO	38	0.572
DWA	31	3.25
Risk Potential	NA (fail)	0.826

Based on the results and analysis, it can be concluded that a suitable avoidance method for vehicles and community roads can be proposed by comparing the original approach with the extended one.

4 CONCLUSIONS

By conducting a comparison of methods using simulations, it was possible to demonstrate the usefulness of the proposed VO-drive approach for autonomous driving on urban roads. After conducting simulations, actual experiments were carried out using a vehicle, and successful avoidance routes were performed.

Three research problems were examined. For the first problem, “many pedestrians are present on community roads”, 2D TTC was used to limit pedestrians performing avoidance in “limitation of the target object” of extension 1. From Fig. 13, it was observed that this limitation delays the avoidance timing, suggesting that avoidance can be performed even in congested situations. For the second problem, the difference between the motion of vehicles and robots, the vehicle dynamics of vehicles were applied in extension 2. This allowed the transition from the conventional two-wheeled model to be restricted to the motion of vehicles. For the third problem, the narrow road width, calculations using the vehicle’s four contour instead of the conventional circular approximation were adopted in extension 3. As shown in Fig. 15, using the vehicle’s contour demonstrated that it is possible to pass through the shortest path without large avoidance maneuvers. This suggests that avoidance can be performed even on narrow roads such as community roads.

5 FUTURE WORKS

Currently, the real vehicle experiments are still ongoing. In the future, it is plan to conduct real vehicle experiments, increasing the vehicle's speed and introducing moving obstacles to create an environment closer to real-life urban road conditions. In addition, by having pedestrians actually walk, it is aim to realize avoidance that makes them feel safe.

Finally, the remaining problem for the practical use of the proposed method are discussed. In the second extension, vehicle motion constraints were considered. However, since the avoidance speed determined here was linearly approximated, the motion was not fully accounted for. Actual vehicle motion is nonlinear. Therefore, it is planned to address this issue by using the bicycle model and conducted real vehicle experiments to perform model identification.

APPENDIX

When calculating the VO region, a comparison will be made between the conventional method of circular approximation and the method proposed in this paper, which uses the vehicle's corner points. In contrast to square robots, vehicles have a rectangular shape. Therefore, when approximating with a circle, unnecessary parts may emerge (refer to Fig. 9). Performing circular approximation on narrow roads, such as community roads, in this state may not provide sufficient space for obstacle avoidance, or there is a risk of avoiding obstacles largely. Therefore, by conducting an approximation from the four corners of the vehicle, it is believed that even large vehicles like cars can navigate narrow roads like community roads while avoiding obstacles. Vehicle corner approximation is shown in Fig. 10.

The discussion will consider simplified shapes of "vertical bar" and "horizontal bar," and subsequently extend to rectangular shapes resembling vehicles.

To begin, it will be examined the case where a vertical bar, representing a simplified shape, is moving and encountering an obstacle of a certain size. The length of the vertical bar in Fig. 18 is taken as $2 \times r_1$, and the obstacle is approximated as a circle with a radius of r_1.

In this scenario, considering that the top and bottom two points of the vertical bar can move as individual points, the resulting VO region can be depicted as shown in Fig. 19.

As the bar is rigid, the top and bottom endpoints cannot move independently. To translate this scenario into one where the velocity obstacle is defined with respect to the center point of the bar, the VO region generated from these two points is shifted to the center of the vertical bar. These two regions, VO_a and VO_b, become the velocity obstacle regions where the endpoints of the bar would collide as it moves. As all points between the top and bottom endpoints lie within the bar, the combined VO_v region encompassing VO_a and VO_b becomes the velocity obstacle region for the entire bar's movement. In this case, the distance from the obstacle to the boundary of the VO_v region is $r_1 + r_2$, where r_1 represents the radius of the vertical bar and r_2 represents the radius of the obstacle (Fig. 20). This is equal to the conventional VO calculation method using circular approximation.

Next, it will be considered a similar analysis for the horizontal bar scenario in Fig. 21.

In this scenario, generating the VO region from two points on the left and right results in the configuration shown in Fig. 22.

Similarly, shift the VO region generated from the two points on the left and right to the center of the horizontal bar. This is illustrated in Fig. 23.

At this point, it becomes evident that the distance from the shifted VO region to the obstacle is shorter than $r_1 + r_2$. This suggests that when approximating with a horizontal bar, the size of the VO region might be smaller compared to the conventional VO calculation method. Let's now verify how much smaller the size of the VO region becomes when compared to the traditional VO calculation method (Fig. 24).

Figure 18 Scenario of vertical bar approximation

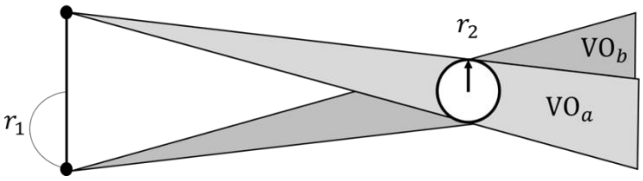

Figure 19 Generation of VO region using vertical bar approximation

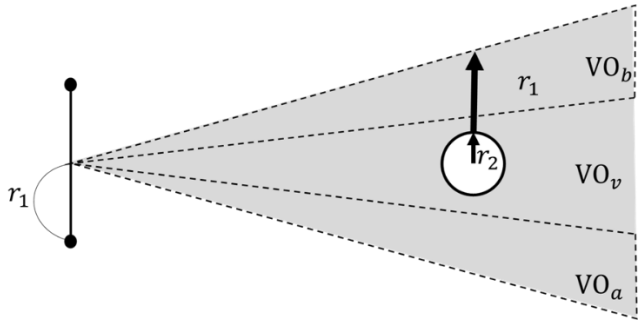

Figure 20 Shifting the VO region to the center of the vertical bar approximation

Figure 21 Scenario of horizontal bar approximation

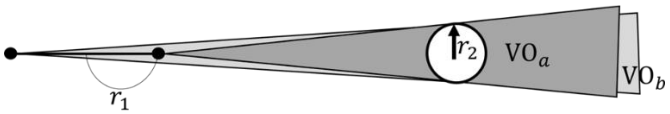

Figure 22 Generation of VO region using horizontal bar approximation

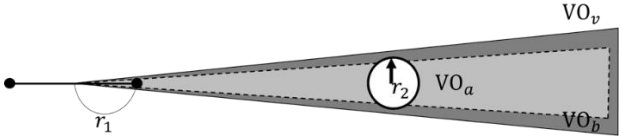

Figure 23 Shifting the VO region to the center of the horizontal bar approximation

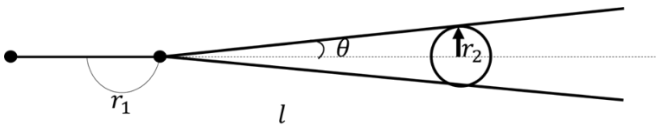

Figure 24 Calculation $\boldsymbol{\theta}$ from the right point of the horizontal bar approximation

Considering the VO region from the right point when approximated by a horizontal bar, as shown in Fig. 24. Here, the angle θ can be expressed as Equation 9.

$$\theta = \tan^{-1}\frac{r_2}{l - r_1} \tag{9}$$

Here, it will be examined how much the VO region generated from the right side of the horizontal bar increases when shifted to the center of the bar (Fig. 25).

Here, when considering the difference $\boldsymbol{d}$ between the VO regions before and after the shift, it can be expressed as Equation 10.

$$d = l \cdot \tan\left(\tan^{-1}\frac{r_2}{l - r_1}\right) - r_2 \tag{10}$$

If the calculated value of $\boldsymbol{d}$ obtained here is shorter than $\boldsymbol{r_1}$, it becomes evident that the resulting VO region will be smaller than the conventional VO region.

Finally, it will be considered the calculations from the corners of the vehicle. It will examine a scenario depicted in Fig. 26.

As mentioned earlier, it has been established that the vertical bar approximation results consistent with the conventional VO method, while the horizontal bar approximation leads to a smaller VO region compared to the traditional method. Based on this, the approach is to calculate the velocity obstacle region in the width direction of the vehicle using conventional circular approximation and then combine this region with the velocity obstacle region in the length direction of the vehicle using a similar method as the horizontal bar approximation (Fig. 27). This way, the overall velocity obstacle region for the entire vehicle can be determined.

For this scenario, the generated VO regions are shown in Fig. 28.

Upon shifting the generated VO regions to the center of the horizontal bar, they transform as shown in Fig. 29.

In this context, the modification in size due to the displacement of the VO regions will be examined.

For the angle θ shown in Fig. 30, it can be expressed Equation 11.

$$\theta = \tan^{-1}\frac{r_1 + r_2}{l - r_1} \tag{11}$$

Subsequently, the difference d between the VO regions before and after the shift, it can be expressed as Equation 12.

$$d = l \cdot \tan\left(\tan^{-1}\frac{r_1 + r_2}{l - r_1}\right) - (r_1 + r_2) \tag{12}$$

Here, a comparison between the proposed method and the conventional circular approximation is conducted. As a method of comparison, the radius of the extended circle from the conventional VO calculation method and the value $d + (r_1 + r_2)$ from the current approach are contrasted. Since the value depends on the distance l from the center of the vehicle

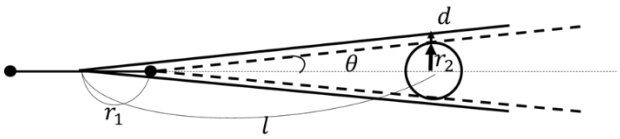

Figure 25 Calculation $\boldsymbol{\theta}$ and $\boldsymbol{d}$ from the center of the horizontal bar approximation

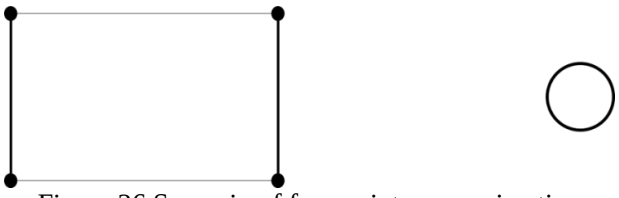

Figure 26 Scenario of four points approximation

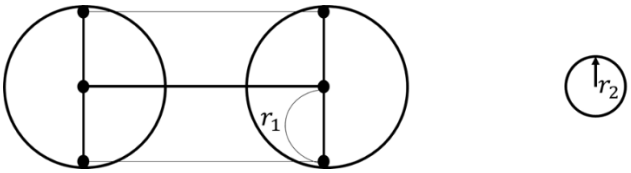

Figure 27 Suggest method to generate VO region

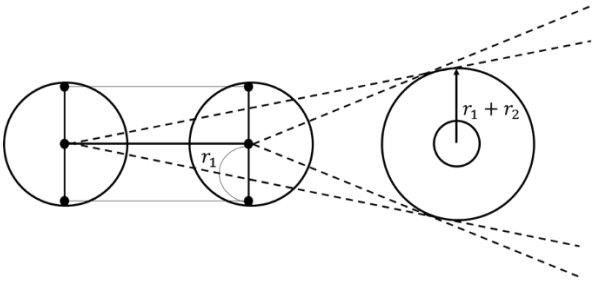

Figure 28 Generation of VO region from suggest method

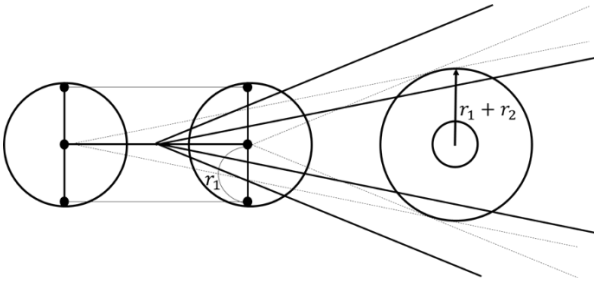

Figure 29 Shifting VO region to the center of the four points approximation

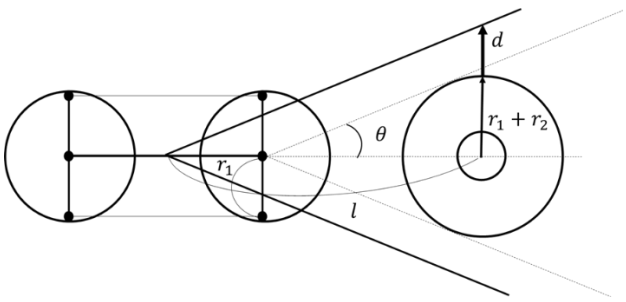

Figure 30 Calculation $\boldsymbol{\theta}$ and $\boldsymbol{d}$ from the center of the four points approximation

to the center of the obstacle, the comparison was carried out by varying the value of l. The radius of the host vehicle r_1 is set to 0.75 m, and the radius of the obstacle r_2 is set to 0.5 m. For simplicity, consider the length of the vehicle as being twice its width. As a result, it was found that for distance less than 1 to 4.9 meters, the conventional circular approximation yields a smaller generated VO region, whereas for distance greater than 4.9 meters, the proposed method leads to a smaller VO region.

So far, assumptions have been made regarding vehicles performing only parallel movements. However, in reality, vehicles not only engage in parallel movements but can also involve rotational motion during navigation. Therefore, navigation in dynamic environments for robots like cars has been developed by David Wilkie and others [15]. The paper introduces the concept of generalized velocity obstacles, aiming to address challenges when utilizing velocity obstacles with kinematically constrained agents such as car-like robots. The formulation is expressed as follows:

$$VO_{(A|B)} = \{\mathrm{v}|\exists t > 0 :: \|A(t,u) - B(t)\| < r_A + r_B \} \quad (13)$$

$$u = arg \min_{u' \notin \cup_{B_i} VO_{(A|B_i)}} \|u^* - u'\| \quad (14)$$

However, because analytical solutions were not feasible, experiments were conducted through simulations. Specifically, additional simulations were conducted to examine the differences in trajectories when the vehicle performs circular evasion around obstacles. In this scenario, the vehicle travels straight from the Start point to the Target point at a speed of 15 km/h, avoiding obstacles. The size of the vehicle in VO-drive simulations was set at a width of 1.5m and a length of 2.13m, and experiments were performed with a radius of 1.357m during VO scenarios. The experiments started with a distance of 25m between the vehicle and the obstacle. For the simulation comparison of differences due to vehicle approximation, 2D TTC was set to 6 seconds for both VO-drive and VO, and self-vehicle trajectory prediction was applied to both. Figure 31 shows the results of the simulation. The upper and lower lines in Fig. 31 represent the road width, set at 5.5m to simulate a community road. As evident from the figure, the proposed method can avoid obstacles while staying within the vehicle width. In contrast, with the conventional circular approximation, it is clear that avoiding within the vehicle width is not achieved. Consequently, it can be inferred that the proposed method performs better in narrow road scenarios when following a straight trajectory.

VO-drive, in contrast to the conventional VO, differs in computational complexity. While the conventional method performs VO calculations from the center of the vehicle, the proposed method calculates VO from the four corners of the vehicle. As a result, the computational complexity of the proposed method is expected to be four times higher than that of the conventional method.

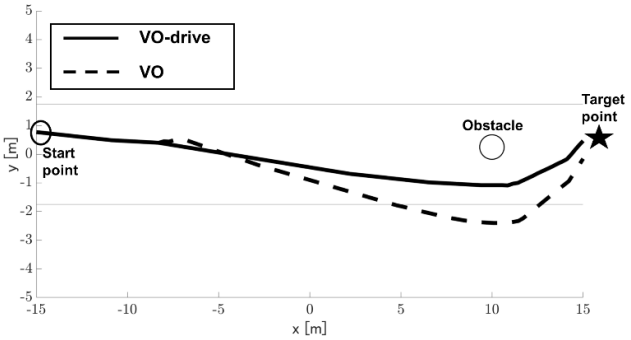

Figure 31 Differences in trajectory by vehicle approximation

It should be noted that the proposed method mentioned above only accounts for parallel displacement. Future work needs to include considerations for rotational movement as well.

REFERENCES

[1] Ministry of Land, Infrastructure, Transport and Tourism, Community road traffic safety measures portal, https://www.mlit.go.jp/road/road/traffic/sesaku/anzen.html.

[2] D. Fox, W. Burgard, S. Thrun, “The dynamic window approach to collision avoidance,” IEEE Robot. Autom. Mag., vol. 4, no. 1, pp. 23-33 (1997).

[3] M. T. Wolf, J. W. Burdick, “Artificial Potential Functions for Highway Driving with Collision Avoidance”, IEEE International Conference on Robotics and Automation (2008).

[4] R. Akabane, Y. Kato, “Pedestrian Trajectory Prediction Based on Transfer Learning for Human-Following Mobile Robots”, IEEE Access, vol. 9, pp. 126172-126185 (2021).

[5] A. J. Sathyamoorthy, U. Patel, T. Guan, D. Manocha, “Frozone: Freezing-Free, Pedestrian-Friendly Navigation in Human Crowds”, IEEE Robot. Automat. Lett., vol. 5, no.3, pp.4352-4359 (2020).

[6] P. Fiorini, Z. Shiller, “Motion Planning in Dynamic Environments Using Velocity Obstacles”, The International Journal of Robotics Research, vol.17, no.7, pp.760-772 (1998).

[7] J. v. d. Berg, M. Lin, D. Manocha, “Reciprocal Velocity Obstacles for Real-Time Multi-Agent Navigation”, IEEE International Conference on Robotics and Automation, pp. 1928-1935 (2008).

[8] J. v. d. Berg, Stephen J, Guy, M. Lin, D. Manocha, “Optimal Reciprocal Collision Avoidance for Multi-Agent Navigation”, IEEE International Conference on Robotics and Automation, pp. 1928-1935 (2010).

[9] M. Gu, Y. Huang, “Dynamic Obstacle Avoidance of Mobile Robot Based on Adaptive Velocity Obstacle”, 36th Youth Academic Annual Conference of Chinese Association of Automation (YAC), pp. 776-781 (2021).

[10] J. D. Jeon, B. H. Lee, “Ellipse-based velocity obstacles for local navigation of holonomic mobile robot”, Electronics Letters, vol. 50, no. 18, pp. 1279-1281 (2014).

[11] Y. Yada, S. Michita, S. Komiya, T. Wakita, “Pedestrian Cooperative Autonomous Mobility -Path Planning Adapted to Pedestrian Face Direction-”, International

Journal of Informatics Society, Vol. 15, No. 1, pp. 43-51 (2023).
[12] M. Abe, Automotive Vehicle Dynamics Trajectory and Applications, Tokyo Denki University Press (2012).
[13] S. Michita, “Autonomous Driving on Community Roads Using Small Mobility – study on Safe Stop Decision –, Kanagawa Institute of Technology, Master’s Thesis (2023).
[14] T. Goto, “Pedestrian behavior prediction and forecast circle generation using Kalman filter”, Kanagawa Institute of Technology, Undergraduate Thesis (2019).
[15] D. Wilkie, J. v. d. Berg, D. Manocha, “Generalized Velocity Obstacles”, IEEE/RSJ International Conference on Intelligent Robots and Systems, pp. 5573-5578 (2009).
(Received: December 15, 2023)
(Accepted: August 22, 2024)

Takumi Seita
He was graduated from school of Vehicle System Engineering, Kanagawa Institute of Technology as a bachelor. Also, he is a master student at Graduate School of Mechanical system engineering, Kanagawa Institute of Technology, Japan. His expertise is development of Autonomous Mobility.

Shunsuke Michita
He was graduated from school of Vehicle System Engineering, Kanagawa Institute of Technology as a bachelor. Also, he earned his master's degree in the Department of Mechanical System Engineering from the Kanagawa Institute of Technology. He is currently employed at Honda Motor Co., Ltd.

Seiji Komiya
He was graduated from the Graduate School of Engineering, Yokohama National University in March 1990. Joined Kanagawa Institute of Technology, where he currently works. His expertise is the development of intelligent mobility.

Toshihiro Wakita received B.E. from Kyoto University, M.S. from The University of Tokyo and Ph.D. degree from Nagoya University in 1983, 1985 and 2006, respectively. He is currently a professor at Kanagawa Institute of Technology. His research interest includes intelligent mobility and human machine interface. He is a member of IEEE, IEICE, and IPSJ.

Regular Paper

Study of an Implementation Method of Point-to-Multipoint Communication for IoT Data Exchange to Reduce Traffic on an IoT Network

Takahiro Shiohara*, Koichi Ishibashi** , and Tetsuya Yokotani**

* Information and Computer Engineering, Graduate School of Engineering, Kanazawa Institute of Technology, Japan
** College of Engineering, Kanazawa Institute of Technology, Japan
k_ishibashi@neptune.kanazawa-it.ac.jp

Abstract - Due to the growing interest in the Internet of Things (IoT) in recent years, platforms for efficiently exchanging IoT data generated by IoT devices such as sensors and actuators among IoT users are being discussed in various areas. In this platform, the interworking among nodal points, which IoT devices and IoT users connect to, is essential to support wide-area and large-scale IoT systems. In addition, it is desirable to share IoT data generated by IoT devices among multiple IoT devices and IoT users in case of notification of alarms, command control to multiple devices, and so on. In address to the above requirements, this paper proposes an implementation method of point-to-multipoint communication to efficiently exchange IoT data among users. The proposed method is characterized by the coordination with multicast control at the application level in order to accommodate various quality of services with IoT data while utilizing Data Distribution Service (DDS). By comparison with the method of using only DDS, it is confirmed that the proposed method reduces the traffic volumes among nodal points and that the transmission latency is suppressed even in an environment where there is a path to a specific node with degraded communication characteristics.

Keywords: Internet of Things, Data Distribution Service, point-to-multipoint communication, IoT Data Exchange.

1 INTRODUCTION

In recent years, there has been growing interest in the Internet of Things (IoT) technology, in which all things are connected to a network. With the expansion and development of IoT-based services and businesses, the number of connected IoT devices is increasing year by year, and IoT devices are expected to exceed 29 billion by 2024[1]. For the increasing number of IoT devices such as sensors and actuators connected to IoT systems, there are many efforts towards developing IoT systems and proposals to efficiently exchange IoT data under wide-area and large-scale IoT networks. For example, there are proposals for monitoring urban transportation systems [2] and research on efficient data collection systems from sensors [3].

In addition, platforms for efficiently sharing data generated by IoT devices (IoT data) among users (IoT users) are also discussed in various places to cope with the growing scale of IoT systems and the increasing number of IoT devices. For example, there is research on providing power-saving IoT services by applying mobile edge computing technology to unmanned aerial vehicles equipped with IoT devices [4]. The IoT data exchange platform (IoT DEP) [5] is another research effort to provide an efficient platform and has been standardized in ISO/IEC 30161 series. In the IoT DEP, IoT end devices, that is, IoT devices and IoT users (servers), access the platform using information centric network (ICN) technologies in order to benefit from high-efficiency communication services. And interoperability among gateways, called nodal points, that accommodate the IoT devices and IoT users is discussed toward the provision of services over wide areas.

Furthermore, in contrast to IoT for consumer fields, applications of IoT in industrial fields have been actively discussed in recent years [6]-[9]. That is, IoT in the industrial fields has strict requirements for reliability and low latency for data, and further research is needed beyond the investigations in IoT for the consumer fields. Also, the short-cycle cyclic communication is a key feature of the industrial applications.

This paper is considering a wide-area and large-scale IoT system for efficient exchanging IoT data among IoT devices and IoT users based on the architecture of the IoT DEP (Fig. 1). That is, our targeted IoT system consists of IoT access networks and an IoT core network. Furthermore, it aims to provide data sharing in point-to-multipoint based communication, such as notification of alarms perceived by IoT devices and command control to multiple devices by IoT users.

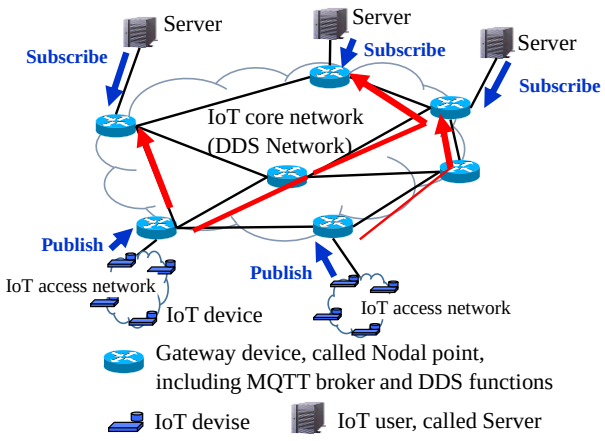

Figure 1: Example of IoT systems.

In the above targeted IoT system, this paper discusses to provide IoT services with various service requirements in terms of point-to-multipoint communications, considering the reliability and low latency data sharing required in the industrial fields. That is, when Data Distribution Service (DDS) is applied to the interconnection among the nodal points on the IoT core network, overheads of control packet by DDS increases, only if the reliable mode provided by DDS is only utilized to achieve interworking among nodal points. On the other hand, interworking based on the best-effort mode provided by DDS is difficult to provide the required service level in the exchange of IoT data with reliability and/or low latency requirements. Therefore, this paper proposes an implementation method which is characterized by the coordination with multicast control at the application level in order to accommodate various quality of services with IoT data while utilizing DDS. It also evaluates the effectiveness of the proposed method.

The remainder of the paper is organized as follows: Section 2 explains the targeted IoT system in the paper. In section 3, related works related to the paper are presented. And, section 4 proposes the implementation method of point-to-multipoint communication at the application level, section 5 describes the results of evaluation. Finally, section 6 concludes the work.

2 TARGETD IOT SYSTEM AND ISSUES

In this section, the IoT system that is the research target of this paper is described and DDS applied in the IoT system is explained. It also describes its challenges.

2.1 Targeted IoT System

Figure 1 shows the targeted IoT system. The targeted IoT system consists of IoT access networks and an IoT core network, called DDS network. The IoT access network is an access network to accommodate IoT devices and IoT users, and is connected to the IoT core network via a gateway device called a nodal point. In the IoT access network, Message Queuing Telemetry Transport (MQTT) [10][11] is deployed as a communication protocol for transmitting/receiving IoT data to/from IoT devices and IoT users. MQTT is a candidate communication protocol for IoT systems. Interworking among multiple MQTT brokers, i.e., nodal points, are coordinated in the IoT core network by DDS [12]. That is, the IoT core network is a network for development of a wide-are IoT system, and multiple MQTT broker, which are implemented on nodal points, are interconnected with each other. The interworking among nodal points is deployed by DDS. DDS is a publish/subscribe communication protocol that supports various communication characteristics and is applied in industrial fields where reliability is required.

IoT data generated by an IoT device is published to a nodal point, which is an MQTT broker. The published IoT data is shared among multiple MQTT brokers because it is utilized by multiple IoT users. In other words, IoT data is forwarded by multicast manner from the nodal point, which the IoT device connects to, to multiple nodal points. IoT data generated by the IoT device require various QoS requirements, such as best effort, reliable, and low latency.

2.2 Data Distribution Service (DDS)

Data Distribution Service (DDS) is data-centric publication and subscription middleware for highly dynamic distributed systems, standardized by OMG (Object Management Group). Data is published to a DDS domain, and subscribers subscribe to share data from that domain without knowing the state of a source node or structure of the information, as shown in (a) of Fig. 2. DDS offers a wide range of Quality of Services (QoS) parameters such as durability, lifetime, presentation, reliability, and delivery time. According to the OMG website, DDS is one of many protocols used in industrial fields such as railway networks, air traffic control, smart energy, medical services, military, and aerospace, and industrial automation.

In a similar way to MQTT, DDS is topic-based publish/subscribe communication, and has in common that the quality control function called QoS can be used to set the guaranteed delivery level and that is implemented by middleware. One difference is that MQTT operates over TCP/IP, while DDS operates over UDP/IP. Another difference in design is that MQTT requires a Broker, whereas DDS does not require a Broker and allows direct communication between Publishers and Subscribers ((b) of Fig. 2). DDS also provides real-time, many-to-many managed connections.

As shown in Fig. 3, the DDS consists of “Real-Time Publish/ Subscribe”, “Minimum Profile” “Durability”, “Ownership”, and Content Subscription”. And the DDS is implemented as an upper layer protocol of UDP/IP, and supports various Quality of Services (QoS) for applications that exchange IoT data through the DDS. A software compliant with the DDS provides application interfaces for transmission and receive of data, such as “DataWriter” and “DataReader” functions. That is, The DataWriter is the application interface and provides a function to transmit data to other nodes. The DataReader is the application interface and provides a function to receive data from other nodes. In the following, the message sequence in providing reliable data exchange is described with reference to Fig. 4. The DataWriter transmits HEARTBEAT packets to support reliable data exchange. That is, The DataWriter transmits a HEARTBEAT to the destination as a packet to confirm the reachability of data with reliable requirements. The DataReader that receives the HEARTBEAT responds with the sequence numbers of the packets it received before receiving the HEARTBEAT. The sender, the DataWriter, confirms that the packet has reached the destination by receiving the response to the HEARTBEAT.

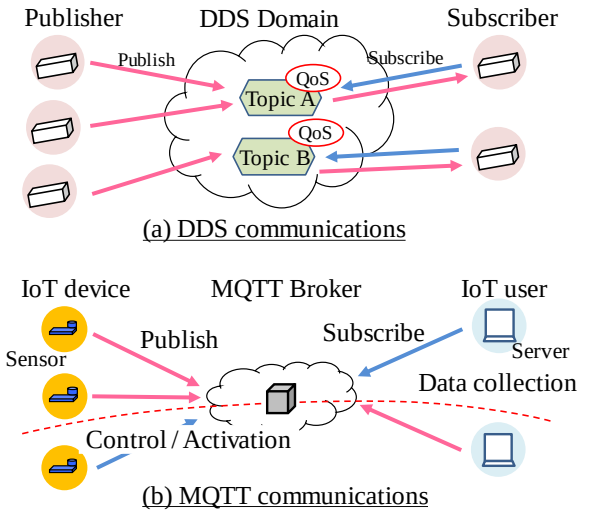

Figure 2: Comparison of DDS and MQTT communications.

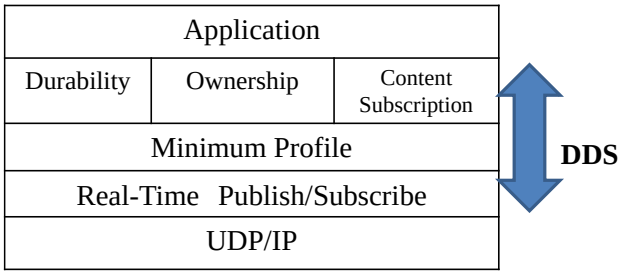

Figure 3: Protocol stack of DDS.

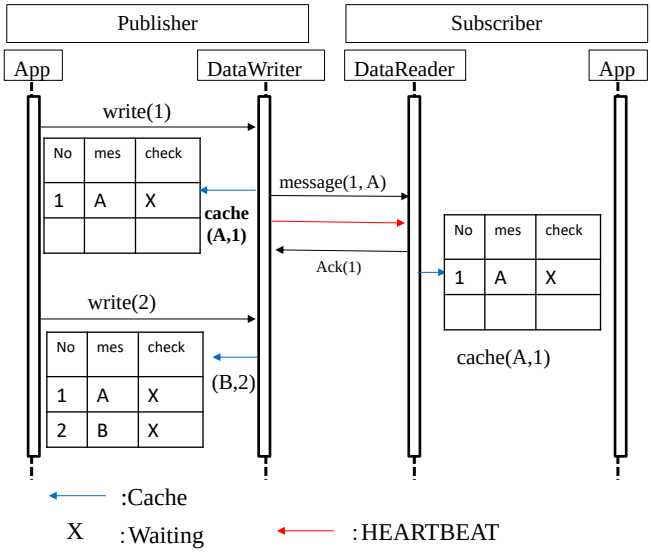

Figure 4: Message sequence of DDS Reliability mode.

2.3 Issues

There are several challenges in developing the targeted IoT systems. In this subsection, several issues related to traffic increase, service level degradation, and information sharing among multiple devices are described. Firstly, the traffic volume forwarded among the nodal points increases as the number of connected IoT devices increases. Secondly, due to the coexistence of IoT data with best-effort requirements on forwarding in the IoT system, there is a degradation of the service level for IoT data with reliable and/or low latency requirements. Lastly, for IoT data that is expected to be shared among multiple IoT devices and IoT users, there is an efficient transfer mechanism to transfer IoT data from a nodal point to other nodal points. Connections between nodal points consist of communication paths with various communication characteristics, and it is necessary to consider the transfer of IoT data to nodal points connected via communication paths with large packet loss and large latency. In other words, in point-to-multipoint communication of IoT data, which requires reliability and low latency, the existing point-to-multipoint communication causes transfer delays due to waiting for arrival confirmation in the worst case, leading to a degradation of the service level. In addition, there is the issue of competition between IoT data requiring low latency and best-effort IoT data at the nodal point.

When DDS is applied in communication among the nodal points, communication services among nodal points depends on DDS functionality. That is, reliability support on DDS is ensured by acknowledgement control from the destination nodes. And, in reliable point-to-multipoint communication on DDS, transmitting of a packet is completed after confirmation of acknowledgements from all destination nodes. Therefore, if there is a nodal point connected via a communication path with large packet loss rate or large latency, point-to-multipoint communication is influenced from the path with large packet loss or large latency. It is necessary to consider a method for ensuring communication methods that does not depend on the DDS functionality and bad communication paths. Based on the above, this paper proposes a multicast control method that considers coordination with DDS by upper-level applications to achieve efficient data communication between DDS functions and IoT data.

3 RELATED WORKS

This section describes the research works related to efforts using MQTT and DDS, and multicast control at the application level.

In [13], several MQTT protocols including the open source “Mosquitto” are evaluated in terms of resource consumption and latency, and the results are shown. In [14], the authors proposed a communication scheme for IoT devices and built a platform for evaluating the system. Evaluations were conducted on a data-by-data basis, showing that the system is efficient in distributing data over a network. In [15], performance evaluation and comparison of communication protocols for IoT such as MQTT and DDS are conducted, and its evaluation shows that MQTT significantly reduces round trip time (RTT) for servers and DDS has high performance in protocol implementation. In [16], data transfer using DDS is implemented, showing that it provides low latency and high throughput, and is an effective communication protocol for communication systems such as those in smart cities.

Regarding the realization of IoT systems using MQTT to deploy large-scale systems, research is being conducted to

evaluate the performance and to propose methods of cooperation with multiple brokers. For example, MQTT systems with multiple brokers have been investigated in many studies [17]-[20]. In [17], MQTT with a spanning tree of brokers on the network (MQTT-ST) is proposed for building a distributed network with multiple MQTT brokers. MQTT-ST enables the data collection from a wide area. However, MQTT-ST has issues such as traffic overhead due to the need for periodic information exchange with the broker.

In [18], a scalable and low-cost MQTT broker clustering system is proposed to handle many IoT devices. In this clustering system, MQTT clients and multiple MQTT brokers are connected by a load balancer to distribute network traffic to the MQTT brokers. Therefore, compared to a single broker, the load on each broker is reduced and the throughput of the entire clustering system is increased, thereby reducing the CPU utilization of each broker.

In [19], MQTT brokers are placed at each network edge to handle data with the characteristic of "edge heavy," where objects at the network edge of an IoT system generate a large amount of data. To coordinate these multiple MQTT brokers, they propose a new mechanism called the ILDM (Interworking Layer of Distributed MQTT brokers). An ILDM node placed between a broker and a client not only relays MQTT clients and brokers as a proxy but also connects to other ILDM nodes to coordinate multiple brokers. Similarly, [20] proposes, implements, and evaluates countermeasures for interworking among MQTT brokers located at the edges of the network.

As shown in [18]- [20], the deployment of systems with multiple brokers is considered in many places for building large-scale systems. However, there are few studies that consider QoS for data shared among MQTT brokers. Therefore, this study considers the deployment of DDS, a publish/subscribe communication protocol that allows the provision of various services including QoS functions and does not require an intermediate node, for interworking among MQTT brokers.

Next, multicast control at the application level is proposed to improve resource consumption, such as throughput, in the target network to address the issues introduced by conventional communication protocols. For example, latency recovery and fault recovery characteristics have been achieved by drastically reducing control traffic in the bandwidth of stagnation [21]. In [22], a protocol for multicasting at the low-bandwidth application layer is proposed to reduce overhead. Simulation evaluations of the protocols implemented in applications show that the proposed protocols can significantly reduce control traffic. In [23], an algorithm is proposed and evaluated to improve end-to-end throughput at the application level. The evaluation results show that the proposed protocol can significantly improve the throughput.

4 PROPOSAL

In this section, a proposed method for efficient IoT data exchange among DDS nodes in the targeted IoT system is described.

The proposed method does not depend on the QoS functions provided by DDS, but implements transmission control functions at the application layer level to provide reliable point-to-multipoint communication with low latency. Although IoT technologies are expected to be applied in various use cases, the QoS functions provided by DDS alone are not sufficient to satisfy a service level required in each use case. Especially in industrial fields, there are demands for short-period cyclic communication and/or low-latency information sharing, which are difficult to be satisfied only by the QoS functions provided by DDS. For example, in [6], the requirements of two type of industrial applications, process automation and factory automation, are described. It shows that requirement for cycle time in a process automation application is 100ms. And in [8], the reliability requirements for process automation applications vary from 10−3 to 10-4 packet loss rate (PLR), while the latency requirements vary from 50 to 100 ms. There is also a scenario in which information generated by a node is shared and distributed to multiple nodes, such as in emergency notification and command control for multiple nodes in an IoT system. Therefore, the provision of low latency and highly reliable communication in point-to-multipoint communication is also a significant challenge.

In order to flexibly support the required communication characteristics for a variety of use cases, this paper proposes an implementation method that implements a transmission control function that achieves communication control corresponding to the required communication characteristics at the upper application layer of the DDS, while using a best-effort type communication mode for DDS due to its low processing. Figure 5 shows the functional architecture on a nodal point, which is a DDS node. Here, the nodal points are the gateways where IoT devices and IoT users connect to, and Fig. 5 illustrates the flow of IoT data when IoT data from IoT devices and IoT users are transferred to the IoT core network side, as arrowed. And, in Fig. 5, IoT data from IoT devices and IoT users are shown as blue lines, and IoT data to the IoT core network side are shown as red lines. The arrows before and after the forwarding application change color because the forwarding application determines the destination of the IoT data. That is, IoT data transmitted by IoT devices and IoT-users via MQTT are notified to the forwarding application in the nodal point via the broker function in the nodal point. The forwarding application receiving the IoT data forwards the received IoT data (message) to the transmission control function, which forwards it to other nodal points via the API provided by the DDS. This application, that is, the transmission control function, implements a transmission control corresponding to the required communication characteristics according to a use case. This paper then implements the transmission control function for the provision of reliable point-to-multipoint type communication and evaluates its effectiveness.

Figure 6 shows an example of the processing sequence for reliable and low latency transmission to multiple destinations in the transmission control function on the nodal point when forwarding IoT data from the IoT device to other nodal points. IoT data from the IoT device are

received on the transmission control function via the MQTT broker and the forwarding application. And the transmission control function forwards received IoT data to other nodal points via DDS protocol by using DDS's API. The communication in DDS is assumed to be a best-effort type service in order to implement QoS control at the application level.

The following describes the operation of the transmission control function. First, the QoS level required by the received IoT data is verified. If the required QoS level is a best-effort service, the received IoT data is forwarded using DDS's API. For IoT data that requires reliability and low latency, the IoT data is copied to the queue corresponding to the destination of the IoT data, and is transferred from each queue in turn. If IoT data remains in the queue, the lifetime of the queued IoT data is confirmed and IoT data that exists exceeding its lifetime is discarded from the queue, and the latest IoT data is queued. When the lifetime of the queued IoT data has not expired, the latest IoT data is queued after the IoT data above. The queued IoT data is discarded when a response is received from the destination.

This enables reliable and low-latency transfer of IoT data to other destinations even when there is a delay or loss in the exchange of IoT data due to a communication path failure with the destination.

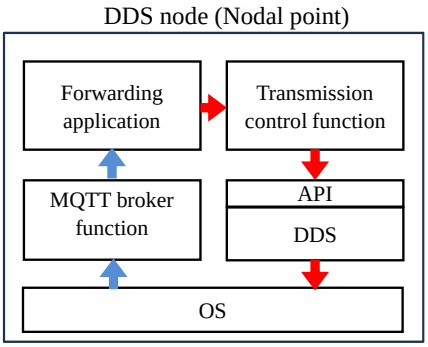

Figure 5: Functional architecture on a DDS node.

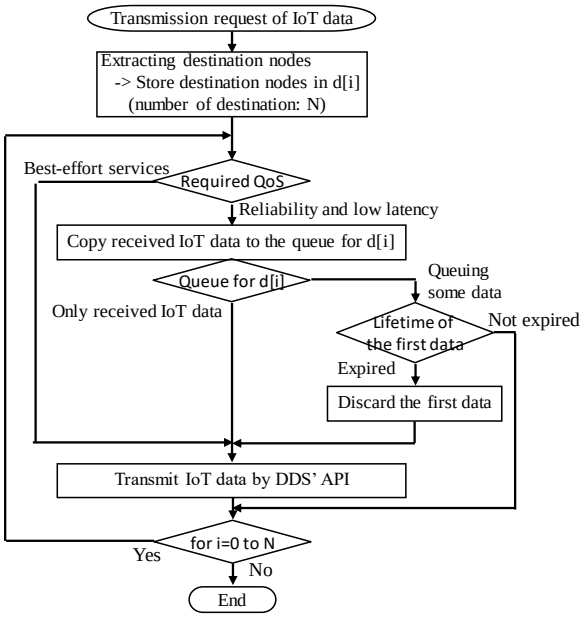

Figure 6: Example of a processing sequence for the transmission control function.

5 EVALUATION

To verify the effectiveness of the proposed method, especially the transmission control function, an experimental network with multiple DDS nodes which is located on nodal points is constructed (Fig. 7). That is, for evaluation, we have developed the experimental environment shown in Fig. 7. In the experimental environment, a Raspberry Pi 4 is used as each DDS node, and the DDS software released by RTI is implemented on the DDS nodes. And the traffic volume between DDS nodes, that is traffic volume on the IoT core network and transmission latency to other nodes are evaluated. In order to emphasize the evaluation of the transmission function, the experimental network consists only of DDS nodes, without IoT devices and IoT-users. In the experimental network, we evaluate the traffic volume when transferring IoT data via the proposed method and via DDS reliability service, called "using only DDS". The traffic volume according to the generation probability of IoT data with reliable and/or low latency requirements are compared with. And, the paper clarifies the effects on transmission latency which is measured from stating of transmission of an IoT data on the publisher side to receiving time of the IoT data on the subscriber sides, to estimate the effect of the degradation of communication characteristics at a specific destination in point-to-multipoint communication on the DDS protocol.

In evaluation of traffic volume on the IoT core network, Node#1 transmits IoT data to other DDS nodes at 1 packet/second in 1000 seconds. And the data transmitted and received on Node#1 are counted. Ratio of IoT data with reliable and/or low latency requirements varied from 10% to 0.5 % (Table 1). It is noted that packet loss of IoT data is generated at uniformly random at a transmission point.

Figure 8 shows the traffic volume when IoT data is transmitted by using the proposed method and by DDS reliability service, called "using only DDS". In Fig. 8, the number of receiving DDS nodes varies from 1 to 5, and ratio of number of IoT data with reliable and/or low latency requirements is configured to be 10%. When "Using only DDS" is applied, the overall traffic volume increased because the traffic of acknowledgment control for confirmation to guarantee the reliability is required for transmitting all IoT data. In the proposed method, the traffic volume is suppressed because acknowledgement is performed at the application level only for IoT data with reliable and/or low latency requirements.

Figure 9 shows the traffic volume depending on the ratio of IoT data with reliable and/or low latency requirements. The number of receiving DDS nodes is configured to be 5 nodes. Ratio of IoT data with reliable and/or low latency requirements varies from 0.5 to 10 %. The traffic volume of the proposed method increases, as the ratio of IoT data with reliable and/or low latency requirements increases. Because in the proposed method, IoT data with reliable and/or low latency requirements require only acknowledgement message. On the other hand, when "using only DDS" is applied, the traffic volume remains constant regardless of the ratio of IoT data with reliable and/or low latency

requirements because reliability service in DDS always checks for transmission acknowledgement.

Next, to evaluate the effect of communication characteristics on the communication path to a specific node, the transmission latency depending on the communication characteristics, such as packet loss ratio, are evaluated. The transmission latency, which is shown in Fig. 12, is defined as the period between the time when a transmission request is issued by the sending node (DDS Node#1 in Fig. 12) and the time when an acknowledgement is received from the receiving nodes (DDS Node#2 to #4 in Fig. 12). It is noted that, in Fig. 12, an case in which an packet loss occurs when transmitting a message to Node #4 is illustrated in order to show the effect on transmission latency when packet loss occurs. Figure 10 and Figure 11 show the transmission latency depending on the communication characteristics (packet loss ratio in the communication path) for the cases 1 and 2 of "2.Transmission latency due to communication characteristics" shown in Table 1. Figure 10 shows the variation of the transmission latency without packet loss in the communication path, i.e., Case 1 of "2.Transmission latency due to communication characteristics" in Table 1. In a stable communication path, the proposed method is not significantly different from the case with using only DDS, even though messages are forwarded to multiple destinations at the application level (Fig. 10). It is assumed that there is a slight delay in DDS due to the "HEARTBEAT" message used to confirm the response.

On the other hand, Fig.11 shows the variation of the transmission latency when packet loss in the communication path to a specific node is observed, i.e., Case 2 of "2.Transmission latency due to communication characteristics" in Table 1. In this figure, IoT data is notified every 50 ms, and the timeout period for the response from the destination node is 50 ms. In Fig. 11, the blue dot when the sequence number of IoT data is 6 indicates the transmission latency between #1 and #2 on the proposed method due to the timeout for the response. The latency is significantly larger than 50msec. However, the latency of the next IoT data, i.e., IoT data with the sequence number of 7, is less than 10 ms, which indicates no effect of the timeout for the IoT data with Sequence number 6. On the other hand, the X dot, when the sequence number of IoT data is 11, indicates the transmission latency between #1 and #2 on the using only DDS due to the timeout for the response. In the case of using only DDS, the latency of the next IoT data with the sequence number of 12 is also affected due to the timeout of the IoT data with the sequence number of 11, which is about 20ms. So, from this figure, it is confirmed that the forwarding in DDS is affected by packet loss in forwarding next IoT data to all destinations. In contrast, since the proposed implementation method implements destination-based retransmission control at the application level, it is possible to confirm that the impact of packet loss is limited to a specific node.

Finally, in order to verify the results of Fig. 8, Fig. 9 and Fig. 11, it clarifies to behavior of message sequences on point-to-multipoint communication under DDS reliability mode. Figure 13 shows the captured message sequences of point-to-multipoint communication from Node#1 (IP address: 192.168.1.1) to Node#2 (IP address: 192.168.1.2) and Node#3 (IP address: 192.168.1.3). It is noted that queue size is configured to be 1 assuming a latency critical application. In Fig. 13, due to the loss of acknowledgements from Node#2, the message requesting an acknowledgement from Node#1, described as "HEARTBEAT" in Fig. 13, continues to be retransmitted. Figure 14 shows the acknowledgement retransmission sequence in point-to-multipoint communications on DDS reliable mode. In this case, since data queue size for retransmission is configure to be 1, the data queue is filled with data to be transmitted to Node#2 and Node#3 by multicast manner due to the packet loss of acknowledgement from Node#2. And the queueing of the next data is blocked. That is, in communications that require an acknowledgement to provide reliability, the delay or loss of response from the specific destination nodes affects the transmission of subsequent packets. This influences the provision of service levels for data with low latency requirements when conflicting with data with various quality requirements.

As described above, the effectiveness of the implementation method for a multicast control coordination scheme in conjunction with DDS has been confirmed through experiments using the experimental environment shown in Fig. 7. In other words, we have evaluated the effectiveness of implementing the reliable control function as a proprietary application for services that require specific reliable and low latency services, as opposed to a general-purpose DDS that supports a wide quality of services. It is noted that there are concerns that implementing a proprietary application outside of the general-purpose DDS imposes an increased processing load and increased latency. However, Fig. 10 shows that the implementation of the reliable control function in a proprietary application does not cause significant processing delays, since the DDS also operates in user space, and latency with the reliable control function is reduced due to the simplification of processing in the DDS. On the other hand, since the implementation of reliable control as a proprietary application is service-specific, there are challenges of adaptability to devices in which a variety of services are required, optimization, and so on.

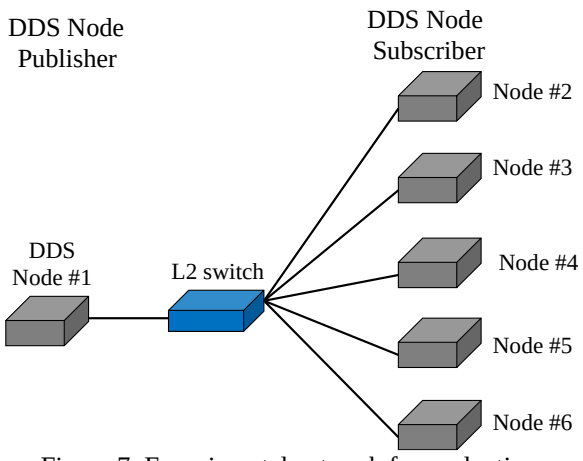

Figure 7: Experimental network for evaluation.

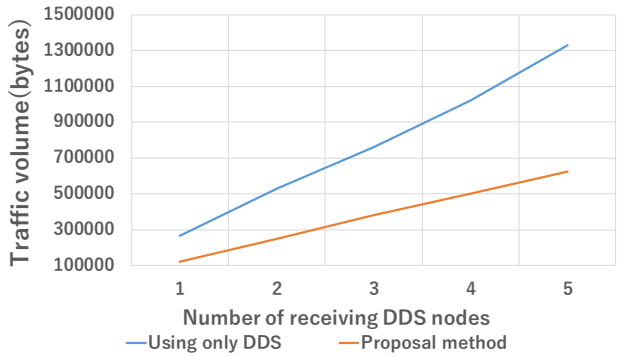

Figure 8: Comparison of traffic on the IoT core network.

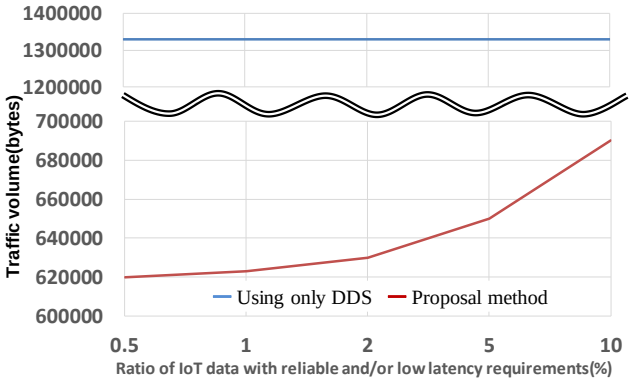

Figure 9: Traffic volume according to ratio of IoT data with reliability and low latency.

Table 1: Evaluation Patterns and Parameters

1. Traffic volume on the IoT core network			
	Case 1	Number of sending nodes	1 (node)
		Number of receiving nodes	1 to 5 (nodes)
		Ratio of IoT data with reliable and/or low latency requirements	10 (%)
	Case 2	Number of sending nodes	1 (node)
		Number of receiving nodes	5 (nodes)
		Ratio of IoT data with reliable and/or low latency requirements	0.5 to 10 (%)
2. Transmission latency due to communication characteristics			
	Case 1	Number of sending nodes	1 (node)
		Number of receiving nodes	1 to 5 (nodes)
		Communication Characteristics (Packet loss ratio)	0.0 (%)
	Case 2	Number of sending nodes	1 (node)
		Number of receiving nodes	1 to 5 (nodes)
		Communication Characteristics (Packet loss ratio)	0.0 to 1.0 (%)

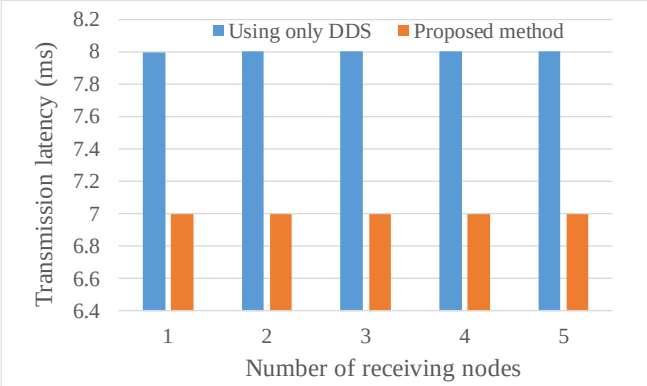

Figure 10: Transmission latency on the proposed method according to number of receiving nodes.

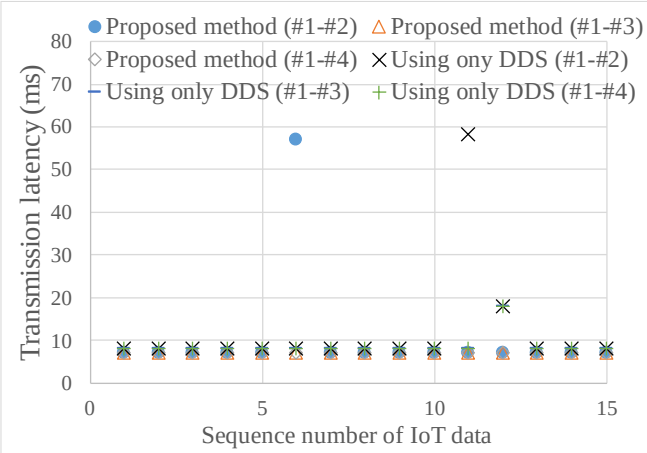

Figure 11: Transmission latency on the proposed method due to packet loss in the communication path to a specific node.

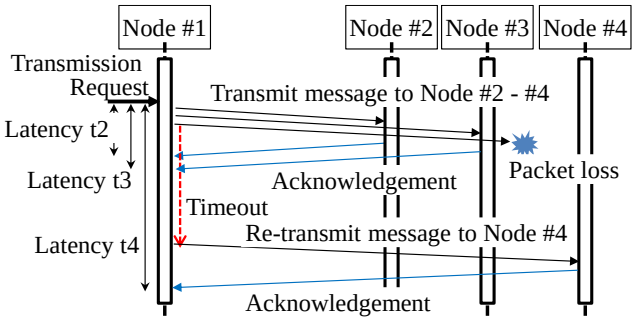

Figure 12: Definition of transmission latency.

192.168.1.1	192.168.1.2	RTPS	49 INFO_TS, DATA
192.168.1.1	192.168.1.3	RTPS	49 INFO_TS, DATA
192.168.1.1	192.168.1.2	RTPS	49,49 INFO_DST, HEARTBEAT
192.168.1.1	192.168.1.3	RTPS	49,49 INFO_DST, HEARTBEAT
192.168.1.3	192.168.1.1	RTPS	50 INFO_DST, ACKNACK
192.168.1.1	192.168.1.2	RTPS	49,49 INFO_DST, HEARTBEAT
192.168.1.1	192.168.1.2	RTPS	49,49 INFO_DST, HEARTBEAT
192.168.1.1	192.168.1.2	RTPS	49,49 INFO_DST, HEARTBEAT
192.168.1.1	192.168.1.2	RTPS	49,49 INFO_DST, HEARTBEAT
192.168.1.1	192.168.1.2	RTPS	49,49 INFO_DST, HEARTBEAT

192.168.1.1: IP address of Node #1
192.168.1.2: IP address of Node #2
192.168.1.3: IP address of Node #3

Figure 13: Packet sequence on DDS reliability mode.

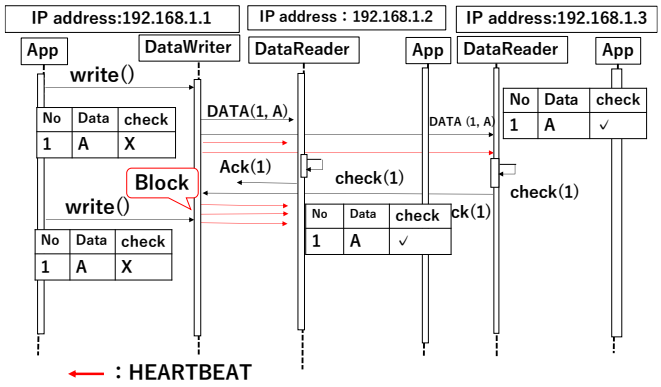

Figure 14: Acknowledgment retransmission sequence in point-to-multipoint communication.

6 CONCLUSION

In this paper, we propose the implementation method for a multicast control coordination scheme in conjunction with DDS as an efficient method of transferring IoT data in IoT systems. We also compared with the data transfer capability of the proposed method and the data transfer using only the DDS function. As results of the evaluation, we confirmed that the proposed method is effective in reducing the traffic volume compared to the communication method using only the DDS function. In addition, we verified the operation in point-to-multipoint in DDS reliability mode. We confirmed that in DDS reliability mode, retransmission for acknowledgement affects transmission of subsequent packets.

In an actual IoT system, various communication characteristics such as packet loss and latency on the communication paths between nodal points are assumed. Therefore, it is necessary to further evaluate the proposed method by considering the communication characteristics of each path in the target IoT system, such as packet loss rate and latency.

REFERENCES

[1] Ministry of Internal Affairs and Communications,"2022 Summary of the State-of-the-Art Report on Information and Telecommunications (in Japanese), " https://www.soumu.go.jp/johotsusintokei/whitepaper/ja/r04/html/nf3r1000.html, Referred in May, 2023.

[2] P. Arman Syah and H. Leslie Hendric Spits Warnars, "Intelligent traffic monitoring system (ITMS) for smart city based on IoT monitoring," 2018 Indonesian Association for Pattern Recognition International Conference. IEEE, pp.161-165 (2018).

[3] A. P. Plageras, K. E. Stergiou, C. Wang, and H. Gupta, "Efficient IoT-based sensor BIG Data collection–processing and analysis in smart buildings," Future Generation Computer Systems Vol.82, pp.349-357 (2018).

[4] M. N. Hossein, M. Bagaa, and T. Taleb, "UAV-based IoT platform: A crowd surveillance use case," IEEE Communications Magazine, vol.55, no.2, pp.128-134 (2017).

[5] T. Yokotani and K. Kawai, "Concepts and requirements of IoT networks using IoT Data Exchange Platform toward International standards", 2019 IEEE Conference on Standards for Communications and Networking (CSCN) (2019).

[6] H. Xu, Wei Yu, D. Griffith, and N Golmie, "A Survey on Industrial Internet of Things: A Cyber-Physical Systems Perspective," IEEE Access, vol. 6, pp.78238-782592018 (2018).

[7] M. Gundall, M. Strufe, Hans D. Schotten, P. Rost, C. Markwart, R. Blunk, A. Neumann, J. Griebbach, M. Aleksy, and D. Wubben, "Introduction of a 5G-Enabled Architecture for the Realization of Industry 4.0 Use Cases," IEEE Access, vol. 9, pp.2169-3536 (2021).

[8] P. Schulz, M. Matthe, H. Klessig, M. Simsek, G. Fettweis, J. Ansari, Shehzad Air Ashraf, B. Almeroth, J. Voigt, I. Riedel, A. Pushmann, Andreas Mitschele-Thiel, M. Muller, T. Elste, and M. Windisch, "Latency Critical IoT Applications in 5G: Perspective on the Design of Radio Interface and Network Architecture," IEEE Communications Magazine, vol. 55, no. 2, pp.70-78 (2017).

[9] C. Paniagua and J. Delsing, "Industrial Frameworks for Internet of Things: A Survey," IEEE Systems Journal, vol. 15, no. 1, pp.1149-1159 (2021).

[10] OASIS Website. (Accessed: October 25, 2023). [Online]. Available:https://www.oasis-open.org/committees/tc_home.php?wg_abbrev=mqtt.

[11] B. Mishra and A. Kertesz, "The Use of MQTT in M2M and IoT Systems: A Survey," IEEE Access, vol. 8, pp.201071-201086 (2020).

[12] P. Bellavista, A. Corradi, L. Foschini, and A. Pernafini, " Data Distribution Service (DDS): A performance comparison of OpenSplice and RTI implementations," 2013 IEEE symposium on computers and communications, IEEE, Vol.2, pp.377-383 (2013).

[13] S. Profanter, A. Tekat, K. Dorofeev, M. Rickert, A. Knoll, "OPC UA versus ROS, DDS, and MQTT: performance evaluation of industry 4.0 protocols," IEEE International Conference on Industrial Technology, pp.955-962 (2019).

[14] B. Melvin, K. Erkin, P. Marc-oliver, and C. Georg. "Open-source mqtt evaluation," 2021 IEEE 18th Annual Consumer Communications & Networking Conference. IEEE, pp.1-4 (2021).

[15] L. Xiangtao, H. Ning, Z.Peng and Z. Yu,"The method of Internet of Things access and network communication based on MQTT." Computer Communications Vol.153, pp.169-176 (2020).

[16] A. Tanushree, N. Payam, M.R.Barzegarn, and V. Luigi. "Multi-level time-sensitive networking (TSN) using the data distribution services (DDS) for synchronized three- phase measurement data transfer," IEEE Access Vol. 7, pp.131407- 131417 (2019).

[17] E. Longo, Alessandro E.C. Redondi, M. Cesana, A. Arcia-Moret, and P. Manzoni, "MQTT-ST: a Spanning Tree Protocol for Distributed MQTT Brokers," 2020

IEEE International Conference on Communications (ICC) (2020).
[18] P. Jutadhamakorn, T. Pillavas, V. Visoottiviseth, R. Takano, J. Haga, and D. Kobayashi, “A Scalable and Low-Cost MQTT Broker Clustering System,” 2017 2nd International Conference on Information Technology (INCIT) (2018).
[19] R. Banno, J. Sun, S. Takeuchi, and K. Shudo, “Interworking Layer of Distributed MQTT Brokers,” IEICE Transactions on Information and Systems, Vol. E102-D, No. 12, pp.2281-2294 (2019).
[20] Y. Noda, S. Ohno, K. Ishibashi, and T. Yokotani, “A new routing mechanism based on layer 2 control in MQTT networks with multiple brokers,” IEICE Communications Express, Vol.11, No.6, pp.307-312 (2022).
[21] L.Jie, Y.Zhou, and H.Chen. "Age of information for multicast transmission with fixed and random deadlines in IoT systems," IEEE Internet of Things Journal, vol.7, no.9, pp.8178-8191 (2020).
[22] B.Suman, B.Bhattacharjee, and C.Kommareddy. "Scalable application layer multicast," Proceedings of the 2002 conference on Applications, technologies, architectures, and protocols for computer communications (2002).
[23] Z.Ying, B.Li,B, and J.Guo. "Multicast with network coding in application-layer overlay networks," IEEE Journal on Selected Areas in Communications, vol.22, no.1, pp.107-120 (2004).

(Received: November 28, 2023)
(Accepted: August 22, 2024)

Takahiro Shiohara received a B.S. degree from Kanazawa Institute of Technology in 2022. He is currently pursuing a M.S. degree at the same university. His research interests include IoT networks and communication mechanisms. He is currently a system engineer in Mitsubishi Electric Corporation.

Koichi Ishibashi received the B.S. and M.S. degrees from Osaka City University in 1989 and 1991 and a Ph.D. degree in communications and integrated systems from Tokyo Institute of Technology in 2017, respectively. He joined the Mitsubishi Electric Corporation in 1991. Since then, he has been engaged in R&D of internetworking equipment, mobile networking, and ad hoc network systems. Moreover, in 2019, he moved to the Kanazawa Institute of Technology as an associate professor. His current research interests include routing technologies for wireless sensor networks and network architectures for IoT.

Tetsuya Yokotani received B.S., M.S., and Ph.D. degrees on information science from the Tokyo University of Science in 1985, 1987, and 1997, respectively. He had worked for Mitsubishi Electric Corporation from 1987, Since then, he has researched high-speed data communication, optical access systems, home network and performance evaluation technologies of networks mainly in the Information Technology R&D Center. He moved to Kanazawa Institute of Technology in 2015, Since then, he has engaged research and education on networks for various IoT services He has been a chair in the IEEE ComSoc the CQR technical committee. Currently, he is a chair of advisory board in this committee. He has also participated in the standardization activities on ITU-T SG15, SG20 and ISO/IEC JTC1. He is also member of IEEE ComSoc and IPSJ, and a fellow member of IEICE.

Regular Paper

A Method for Estimating Bicycle Air Pressure Decrease based on Vibration Sensing of Bicycles using Smartphone

Rui Yamaguchi† and Katsuhiko Kaji†

†Graduate School of Business Administration and Computer Science, Aichi Institute of Technology

{b23724bb, kaji}@aitech.ac.jp

Abstract - Some people experience accidents or near misses while riding because they did not conduct bicycle inspections before riding. There is a need to promote riders to conduct bicycle inspections to reduce the number of people who experience this. In this study, we focus on air pressure inspection and propose a method for estimating bicycle air pressure decrease based on vibration sensing using smartphone. The acceleration in the direction perpendicular to the ground is acquired with a smartphone, and the standard deviation and the amplitude spectrum of each frequency are used as features to estimate the air pressure decrease using random forests and other methods. Evaluation experiments were conducted to classify whether the best timing for tire inflation, to estimate the air pressure value and classify it based on that value, and to evaluate whether the training data from other locations and bicycles can be diverted. The results of the evaluation experiments showed that 96.1% correctly classified when tire inflation was needed, but it was difficult to divert the training data. We developed an application that promotes air pressure inspection using the proposed method.

Keywords: Smartphone, Sensor signal processing, Bicycle, Air pressure

1 INTRODUCTION

There is a need to promote bicycle inspections because only a few people who ride a bicycle do so every time. According to a survey conducted by au Insurance, 86.9% of bicycle riders do not conduct any or few necessary inspections before riding(whether the brakes work, whether the tires are inflated sufficiently, the position, color, and angle of reflective materials, whether they are dirty, whether the handlebars and saddle are not wobbly, whether the chain is loose or rusty, whether the bell and buzzer ring, whether the lights come on) [1]. 89.3% of bicycle riders do not conduct annual bicycle inspections at a bicycle store. According to Bicycle Association, it is recommended that you conduct your bicycle inspections every time you ride your bicycle, and that they conduct bicycle inspections at bicycle stores at least once every six months [2]. 81.8% of bicycle riders experienced bicycle malfunctions without inspections. One in five of them experienced accidents or near misses. There is a need to promote riders to conduct bicycle inspections before riding to reduce the number of malfunctions and accidents or near misses experience.

In this study, we focus on tire air pressure inspection among the inspections that should be conducted before riding, and the purpose of this study is to realize air pressure inspections without introduction / operation costs and time consuming. Existing inspection methods need to use exclusive devices such as air gauges to confirm air pressure. Even with exclusive devices, there is a need to remove the cap from the valve of the tire in order to measure it. This method is time consuming.

In this study, a method for estimating air pressure decrease using smartphone is proposed. There is need for a sensor to estimate air pressure decrease. Smartphones are equipped with many sensors. There is no need to purchase new sensors because smartphones are widely used nowadays. In addition, they can quickly confirm the results of air pressure estimation because they are often carrying their smartphone with them at all times. For these reasons, we considered that air pressure inspections could be promoted using smartphone without introduction / operation costs and time consuming.

The flow of promoting air pressure inspection using smartphone is shown in the Fig. 1. The rider inflates the tire to the maximum proper pressure indicated on the side of the tire. Next, the rider rides bicycle while in possession of a smartphone. The smartphone collects feature values that occur at the best timing for tire inflation using equipped sensors. The smartphone estimates whether the air pressure is the best timing for inflation. The best timing for inflation is when the air pressure is about to decrease below the minimum proper pressure. The minimum proper pressure is the minimum pressure that can make the tire perform effectively. The smartphone promotes the rider to inflate when it estimates the best timing for inflation. In this flow, There is no need to confirm the air pressure frequently or to use exclusive devices to measure it. Therefore,we consider that air pressure inspection can be conducted without installation/operation costs and time consuming.

The outline of this study is as follows. Chapter 2 introduces air pressure related works, and describes their features and problems. Chapter 3 describes a method for estimating air pressure decrease based on vibration sensing of a bicycle using a smartphone in order to solve the problems of existing methods. Chapter 4 evaluates the method proposed in this study, and Chapter 5 considers the results. In conclusion, a summary and future issues are describes.

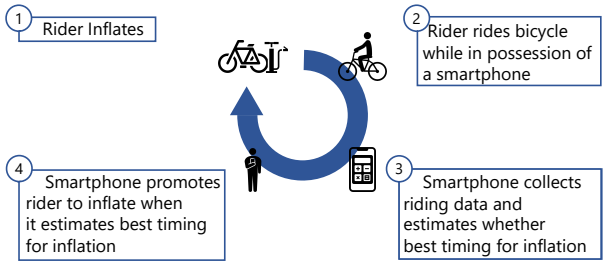

Figure 1: Flow of promoting air pressure inspection using a smartphone

2 RELATED WORK

In this chapter, studies using sensor data for situation estimation, studies using smartphones as a sensing terminal, and existing products related to air pressure inspection, and studies related to air pressure are introduced. The features, advantages, and problems of these studies and existing products are then described.

2.1 Studies Using Sensor Data for Situation Estimation

There are studies on situation estimation using sensor data to estimate road surface conditions [3], [4]. In these studies, data acquired from accelerometers [3] and cameras [4] are used to estimate the situation. Also, there is a study that uses Wi-Fi to detect changes in the state of indoor doors and windows [5]. This sutdy use data acquired by sensors to estimate the situation of places and objects.

It is time consuming to confirm a situation in multiple places or multiple times by visual confirmation. As an example, describe the case of visual confirmation of road surface condition. If there are multiple places to confirm, there is time consuming to move to a different place. If there are multiple times to confirm, there is a need to go to confirm at a certain time. Using the sensor, data collected at a certain time at the confirmed places can be estimated for the road surface condition. Therefore, road surface conditions can be estimated by the sensors without time consuming. Similarly, we considered that tire air pressure inspection could be conducted by sensors without time consuming.

2.2 Studies Using Smartphones as Sensing Devices

There are studies that use smartphones as sensing devices for congestion sensing [6]. A general smartphone is equipped with various sensors such as acceleration sensor, gyro sensor, magnetic sensor, GPS, barometric sensor, proximity sensor, light sensor, camera, and microphone. Therefore, a single smartphone can acquire multiple sensor data. The smartphone is widely used nowadays, and many people are often carrying their smartphone with them at all times. Therefore, estimation using smartphone is without introduction / operation cost. In some cases, a system is created using multiple exclusive sensors. Using the system, there is a need to use multiple exclusive sensors as well. A system using smartphone as a sensing device can be easily used. If the system is released to the application store, it can be used by many people who have smartphone. Because of these advantages, we considered that we could take advantage of them in this study.

2.3 Existing Products Related to Air Pressure Inspection

There are products that help to confirm air pressure such as air pressure sensor from Kashimura [7] and Tyrewiz from Quarq [8]. The air pressure sensor from Kashimura [7] is attached to four tires of a car. The air pressure information is wirelessly transmitted to a monitor in the automobile. The air pressure is displayed on a monitor in real time. Tyrewiz from Quarq [8] is attached to two tires of a bicycle. The exclusive application is installed on a smartphone. The air pressure information is wirelessly transmitted to a exclusive application. The air pressure is displayed on a exclusive application in real time. The rider can always confirm the air pressure. Therefore, there is no time consuming to confirm the air pressure. However, exclusive sensors are expensive and there is a need to manage batteries. Therefore, installation / operation costs are high. In this study, Smartphone is used as a sensor. There is no introduction and operation cost with this method.

There is a product that helps to inflate such as Smart Air Inflator from KuKiire [9]. When the inflator is attached to the tire, it automatically inflates the tire. The air pressure can be automatically inflated to the preferred pressure at the time of inflation. Therefore, there is no time consuming process to conduct air inflation. However, this product does not always measure air pressure. Therefore, if the rider determines that there is no problem in dangerous condition, the rider will ride in a dangerous condition. In this study, the smart phone estimates the best timing for inflation. Dangerous riding conditions are prevented for this method.

There is product that does not require air pressure such as Air Free Concept from Brigestone [10]. A tire that does not require air is called a punctureless tire. When regular tires are replaced with punctureless tires, there is no need for air pressure inspection without time consuming. However, punctureless tires cost more than regular tires. In addition, the ride quality is different between regular and punctureless tires, and the rider feels uncomfortable. In this study, bicycles used in everyday life will be used. The ride quality is not affected for this method.

2.4 Studies on Air Pressure

There are studies on air pressure such as TPMS. TPMS is a air pressure monitoring system using a barometric sensor. TPMS are broadly classified into direct and indirect methods.

There is a direct method study that proposes a technology to improve the performance of barometric sensors [11]. A barometric sensor is directly attached to the tire and measures the air pressure. Therefore, air pressure can be measured

with high accuracy. However, barometric sensors are expensive to produce.

There is a indirect method study that uses a single barometric sensor to estimate the air pressure of four tires [12]. One barometric sensor measures the air pressure of one tire. The air pressure of one tire is used to estimate the air pressure of the other three tires. If the air pressure of four tires is to be measured directly, there are need to use four barometric sensors. However, only one barometric sensor is used to estimate air pressure. Therefore, air pressure estimation can be conducted at low cost. However, a dedicated sensor is used even if only a little. Therefore, it is costly to a certain extent.

In a previous study, we examined air pressure decrease estimation from bicycle riding speed [13]. The force required to pedal decreases as air pressure decreases. Therefore, we considered that the riding speed would decrease as well. An experiment was conducted to estimate air pressure decrease using riding speed. From the results, features that can be estimated for air pressure decrease did not occur. As the reason for this, features that can be changed by the rider's discretion were used. For example, even hen the pedals felt heavy, the rider adjusted the force and drove at the same speed as when there was enough air pressure. Therefore, there is a need to use features that occur with air pressure decreases that the rider cannot change.

3 METHOD FOR ESTIMATING AIR PRESSURE DECREASE BASED ON VIBRATION SENSING

This chapter describes the proper pressure required for air pressure decrease estimation. Then, the flow of air pressure decrease estimation using vibration is described.

3.1 Proper Pressure

There is a proper pressure for effective tire performance for bicycles. The maximum value of the proper pressure is referred to as the maximum proper pressure. The minimum value of the proper pressure is referred to as the minimum proper pressure. If the pressure is within the proper range, it indicates for effective tire performance. If the rider continues to ride outside of the proper pressure, the tire will suddenly burst, and the tube inside the tire will deteriorate. Therefore, air pressure inspection is important to prevent tire burst and deterioration. There may be a maximum proper pressure indicated on the side of the bicycle tire as shown in the Fig. 2. Also, there may be a maximum and minimum proper pressure indicated on the side of the bicycle tire. For city bicycles, only the maximum proper pressure is often indicated. For road bicycles, the maximum and minimum proper pressure are often both indicated.

When the air pressure is about to decrease below the minimum proper pressure, this is the best timing to inflate. If the air pressure is more than the minimum proper pressure, there is no problem to ride. If the air pressure is less than the minimum proper pressure, it is dangerous to ride. Therefore, there is a need to promote inflation to the rider when the air pressure is about to decrease below the minimum proper pressure.

Figure 2: Maximum proper pressure indicated on the side of the tire

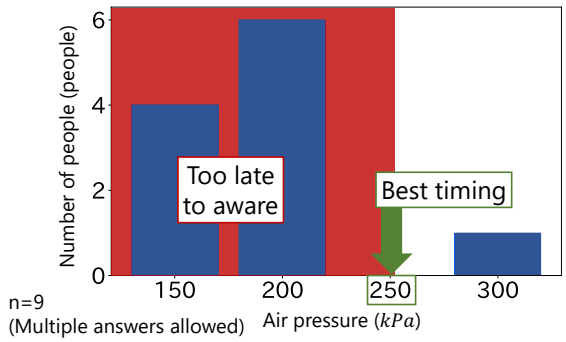

Figure 3: Air pressure that subjects felt should be inflated

3.2 Necessity of Air Pressure Decrease Estimation

Preliminary experiment was conducted to confirm that there is a need for air pressure decrease estimation. Nine male undergraduate and graduate students were asked if they felt they should be inflated. Subjects were asked to ride bicycles at 50 kPa increments from 150 kPa to 300 kPa without informing the air pressure. Subjects were then asked when they felt they should be inflated. Multiple answers were allowed when they felt they should be inflated. The subjects were also divided into two groups. The experiment was conducted by changing the order of air pressure for each of the two groups.

The results of the preliminar experiment are shown in the Fig. 3. Many subjects felt that they should be inflated at 200 kPa and 150 kPa. The minimum proper pressure for the bicycle used in this study is 250 kPa. Therefore, 250 kPa is the best timing for inflation. However, many people do not inflate at the best time and ride in dangerous conditions. From the result, it was found that there is a need to inform the rider of the best timing for inflation.

3.3 Flow of Air Pressure Decrease Estimation Using Vibration

Bicycle vibration was used as a method to estimate the best timing for inflation. Bicycle vibration changes depending on air pressure. A schematic diagram of vibration changes as-

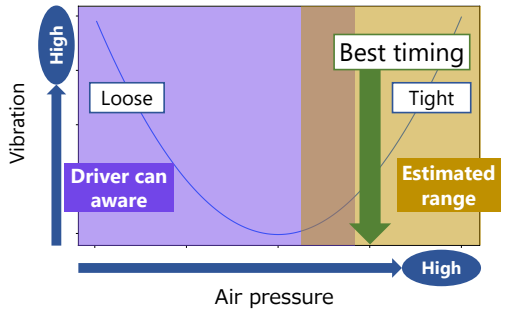

Figure 4: Schematic diagram of vibration changes associated with changes in air pressure

sociated with changes in air pressure is shown in the Fig. 4. If the air pressure is high, vibration is not absorbed very well. If the air pressure decreases to a certain degree, vibration is absorbed by the increased cushioning. If air pressure decreases significantly, vibration is not absorbed by the decreased cushioning. However, the rider can clearly aware that the condition is dangerous. Therefore, we conduct the estimation to the range where the rider does not aware that the condition is dangerous.

The flow of estimating air pressure decrease using vibrations is shown in Fig. 5. The flow consists of preparation and sensing, feature extraction, and air pressure decrease estimation by machine learning.

The rider enters the minimum proper pressure for the bicycle into the smartphone. The minimum proper pressure is necessary to acquire the best timing for inflation.

The rider attaches the smartphone as shown in the Fig. 6 and rides on a paved road. The smartphone is attached to the bicycle so that it is perpendicular to the ground using a smartphone holder. The smartphone must not obstruct the driving. Therefore, the smartphone conducts sensing without displaying the screen. Vibration changes depending on the ground type ridden on. Therefore, the estimation is conducted on paved roads that are generally used. Also, the vibration changes during a stop at a signal and with bumps. When stopped, the vibration is not changed by the air pressure. Vibration changes from different bumps. Therefore, data from such situations are excluded, and sensing is performed in situations where it is easy to estimate.

Acceleration in the y-axis direction during riding can be used as the vibration generated by the contact between the ground and the tires when the smartphone is attached as shown in the Fig. 6. However, the gravity acceleration is also included in the acceleration in the y-axis direction. Therefore, the acceleration in the y-axis direction without the gravity acceleration, is used.

Features of air pressure decrease are extracted from the acceleration data acquired during riding when the rider arrives at the destination. The standard deviation of acceleration in the y-axis direction and the amplitude spectrum for each frequency are used as the feature values. The acceleration standard deviation in the y-axis direction is considered to indicate the strength of the bicycle vibration. Also, the amplitude spectrum of each frequency in the y-axis direction is considered to be a distribution of frequencies of the vibration occurred in the riding. Air pressure decreases as tire cushioning increases within the estimated range. Therefore, it is considered that the vibration of the bicycle is decreased and the acceleration standard deviation is decreased. In addition, it is considered that the vibration at higher frequencies is absorbed and the higher frequency amplitude spectrum is decreased. Therefore, we considered that the acceleration standard deviation in the y-axis direction and the amplitude spectrum for each frequency could be used as features for air pressure decrease estimation.

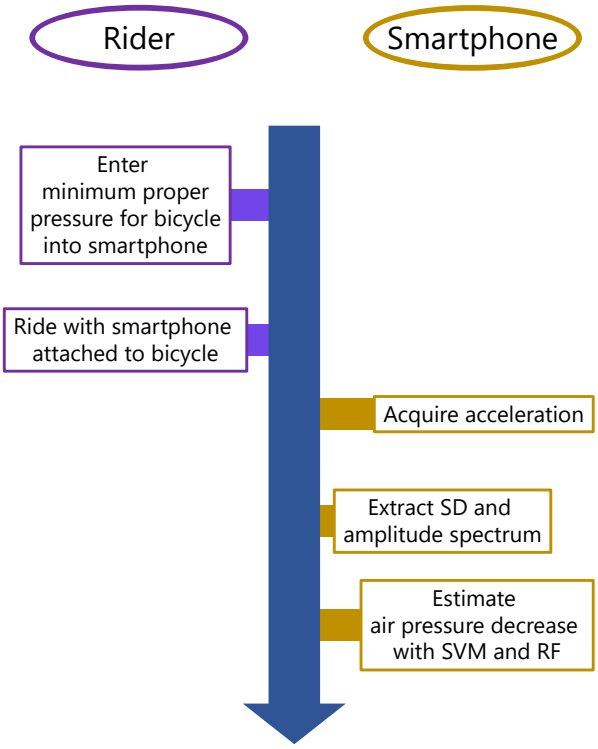

Figure 5: The flow of estimating air pressure decrease using vibrations

Preliminary experiment was conducted to confirm whether the standard deviation of acceleration in the y-axis and the amplitude spectrum of each frequency can be used as fea-

Figure 6: Smartphone attached and acceleration axis

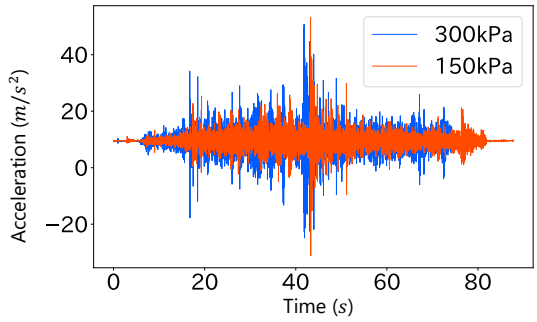

Figure 7: Acceleration in y-axis direction for each air pressure

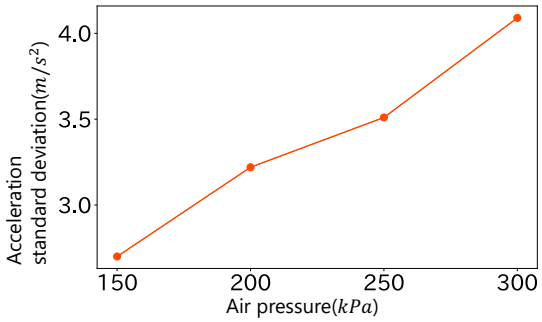

Figure 8: Variation of mean acceleration standard deviation in y-axis direction for each air pressure

tures for air pressure decrease estimation. The experiment was conducted with nine male undergraduate or graduate students. A smartphone was attached to the bicycle as shown in the Fig. 6. Subjects were asked to ride bicycle at 50 kPa increments from 150 kPa to 300 kPa for pressure and the acceleration in the y-axis direction was acquired. The acceleration in the y-axis direction was acquired as shown in the Fig. 7. The standard deviation was acquired from the acquired acceleration in the y-axis direction without the gravity acceleration. The acceleration standard deviations of the nine persons were averaged, and the variation of the values for each air pressure is shown in the Fig. 8. The standard deviation of acceleration in the y-axis direction decreases as the air pressure decreases, and a trend similar to that within the estimated range shown in the Fig. 4 occurs. FFT (Fast Fourier Transform) was conducted on the acceleration in the y-axis direction in order to analyze the frequency components in the y-axis direction. The amplitude spectrum for each frequency in the y-axis direction is shown in the Fig. 9. A trend that the amplitude spectrum with higher frequencies decreases as air pressure decreases occurred. Therefore, the standard deviation of acceleration in the y-axis direction and the amplitude spectrum for each frequency were used to estimate the air pressure decrease.

Machine learning is conducted using the features to estimate whether the air pressure is about to decrease below the minimum proper pressure. The data set format of the features is shown in the Table 1. Explanatory variable is the standard deviation of acceleration in the y-axis direction and the amplitude spectrum for each frequency. The objective variable is air pressure. Amplitude spectrum for each frequency uses the

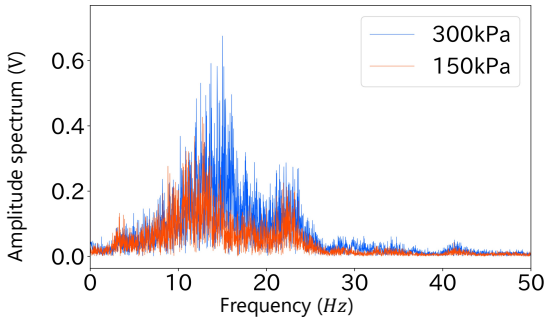

Figure 9: Amplitude spectrum for each frequency generated by bicycle riding

Table 1: Dataset of air pressure decrease features

Explanatory variable		Objective variable
Acceleration standard deviation in y-axis direction (m/s^2)	Amplitude spectrum in y-axis direction (V)	Air pressure of tire (kPa)

average of 0.5 Hz intervals of the frequency. Areas where no significant change occurred when air pressure decreased were not used as features. From the Fig. 9, little change in frequency was occurred after 40Hz. Therefore, the amplitude spectrum in the range of 0.0Hz to 40.0Hz was used. The reason for this narrowing of the range is that a larger amount of data would be burdensome to process on a smartphone. A model trained on this data set is used to classify whether the air pressure is below the minimum proper pressure. There are methods of direct classification using SVM and other methods. Another method is to conduct a regression to estimate air pressure as a numerical value using a random forest or other methods and then classify the air pressure.

4 EVALUATION EXPERIMENT

Experiments were conducted to evaluate the method proposed in this study and air pressure decrease estimation at other locations and on bicycles. The evaluation experiment of the proposed method is designated as Evaluation Experiment 1. The evaluation experiment of air pressure decrease estimation at other locations and on bicycles is designated as Evaluation Experiment 2.

4.1 Evaluation of Air Pressure Decrease Estimation Using Vibration

We conducted Evaluation Experiment 1. The purpose is to evaluate the accuracy of the results estimated by machine learning classification and regression using the standard deviation of acceleration in the y-axis direction and the amplitude spectrum for each frequency.

The experimental setting is shown in Table 2. The subjects were nine male undergraduate or graduate students. The sensing terminal was Galaxy Note 9. The smartphone application phyphox was used to acquire sensor data. The sam-

pling frequency of acceleration is 400 Hz. The location used for the experiment is shown in the Fig. 10. The location is defined as location A. The experiment was conducted on an all paved road so that changes in the road surface would not affect the vibration. In addition, the experiment was conducted on single road without congestion so that the rider did not have to stop. The bicycle used for the experiment is shown in the Fig. 11. The bicycle is defined as bicycle X. In this study, the target is people who use bicycles only for transportation purposes and have little interest in bicycles. People who have little interest in bicycles often use city bicycles which can be purchased inexpensively. Therefore, city bicycle was used in the experiment. The air pressure used for the experiment is 50 kPa increments from 150 kPa to 300 kPa. When the air pressure is 150 kPa, the rider is aware that the air pressure is low. 300 kPa is the maximum proper pressure for the bicycle. The bicycle valve used in the experiment is shown in Fig. 12. The valve shown in the ^^c2^^a0Fig. 12a is called English valve. It is difficult to measure air pressure correctly with English valve. Therefore, English valve was converted to American valve. American valve is shown in the Fig . 12b. It is possible to measure air pressure correctly with american valve. The bicycle used in the experiment was not indicated with the minimum proper pressure. When the weight percentage of the front and rear wheels is the same and the road is paved, the minimum proper air pressure is obtained by the Formula (1)[1]. The bicycle information shown in the Table 3. The weight is defined as 65 kg which is the average weight of a male in his 20s. From the Formula (1)[1], the minimum proper pressure was 250 kPa. Nine subjects rode back and forth along a single road at four different air pressures. A total of 72 data were collected. SVM and Random Forest were used for classification. Random Forest was used for regression. The evaluation was conducted using leave-one-out in which one person's data was the test data from the entire data. The correct rate is the probability that the actual pressure and the estimated result could be classified in the same way. Recall rate is the probability that the estimated result could be classified as not proper when the actual air pressure is out of proper. The correct rate and the recall rate were used to evaluate the results. The accuracy of estimating whether a situation is dangerous or not is important. Therefore, the evaluation was based on the accuracy of the judgment, not on the accuracy of the numerical values obtained in the regression.

The results were shown in the Table 4,5,6,7. The ○ marks indicate the training score when the feature is used. The evaluation results showed higher scores when only the amplitude spectrum of each frequency was used and when both the acceleration standard deviation and the amplitude spectrum of each frequency were used as features. In classification, the correct response rate was 88.9% and the recall rate was 91.1%. In regression, the correct response rate was 79.2% and the recall rate was 96.1%.

[1]Bicycle Exploration!
https://jitetan.com/tire_air_pressure.html

Table 2: Setting of Evaluation Experiment 1

Number of subjects	9
Sensing terminal	Galaxy Note 9
Sampling frequency	400 Hz
Location	Paved road without congestion
Type of bicycle	City bicycle
Air pressure	150 kPa to 300 kPa
Number of data	72
Evaluation method	Leave-one-out
Evaluation index	Correct and recall

Figure 10: Location of Evaluation Experiment 1

4.2 Evaluation of Air Pressure Decrease Estimation at Other Locations and Bicycles

We conducted Evaluation Experiment 2. The purpose is to confirm whether air pressure decrease estimation can be conducted using data from other locations or bicycles.

The experimental setting is shown in Table 8. This subject was the first author of this study. The same location A as in Evaluation Experiment 1 was ridden by another bicycle, another location was ridden by the same bicycle X as in Evaluation Experiment 1, and another location and bicycle were ridden at the same location as in Evaluation Experiment 1. The locations used as different locations from Evaluation Experiment 1 are shown in the Fig. 14. The left location is defined as location B and the right location is defined as location C. A flatter road was chosen as a difference from the location of Evaluation Experiment 1. The bicycles used as different bicycles from Evaluation Experiment 1 are shown in the Fig.

Figure 11: Bicycle X of Evaluation Experiment 1

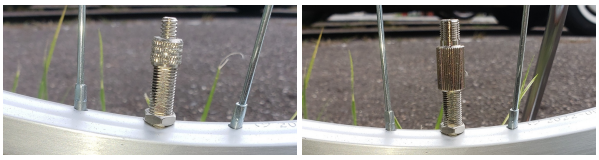

(a) English valve **(b)** American valve

Figure 12: Valve style of bicycle tire

Table 3: Information on the bicycle used in the Evaluation Experiment 1

Bicycles	Weight	Tire width	Minimum proper pressure
X	20.5kg	35mm	250kPa

15. The top bicycle is defined as bicycle Y and the bottom bicycle is defined as bicycle Z. As in Evaluation Experiment 1, The bicycles used in the experiment were not indicated with the minimum proper pressure. The bicycle information shown in the Table 9. From the Formula (1)[1], the minimum proper pressure of bicycle Y is 240 kPa and that of bicycle Z is 230 kPa. The subject rode twice back and forth on a single road at three different locations, on three different bicycles at four different air pressures. A total of 48 data were collected. From the results of Experiment 1, some degree of accuracy was confirmed in the regression. Therefore. Random Forest was used for regression. The regression can acquire numerical results of the estimation. Numerical values provide more evidence for inflation. The sensing terminal and air pressure range are the same settings as in the Evaluation Experiment 1.

The results are shown in the table 10. The figure shows the correct and recall rates for each location and bicycle using the data trained on location A and bicycle X used in the Evaluation Experiment 1. The second row from the top shows the correct and recall rates for the same conditions as the training data. Both the correct rate and the recall rate were low for a different location from the training data and for a different bicycle. Both the correct rate and the recall rate were low for the same location as the training data and for a different bicycle. In the case of the same bicycle, at a different location, the recall rate was higher, but the correct rate was lower.

5 DEVELOPMENT OF APPLICATION USING PROPOSED METHOD

We developed an application to promote air pressure inspection in order to make it possible to realize air pressure inspections without introduction / operation costs and time consuming. Using the proposed method, we estimated the air pressure and determined whether it was dangerous or not.

$$mpp = 10 \times \text{round}\left(0.5 \times 10 \times \frac{0.9}{tw - 11.2} \times (bow + biw + 46)\right) \quad (1)$$

Symbol	Description
mpp	Minimum Proper Pressure $[kPa]$
tw	Tire Width $[mm]$
bow	Body Weight $[kg]$
biw	Bicycle Weight $[kg]$
round(x)	Rounding off x

Table 4: Correct rate of each feature in the classification

Used feature values		Correct rate(%)	
Acceleration standard deviation	Amplitude spectrum for each frequency	SVM	RF
○	○	88.9	83.3
○		72.2	68.1
	○	86.1	84.7

An application that promotes air pressure inspection using the proposed method is shown in the Fig. 16. There is a training state and an estimation state.

It begins with a training state in which data is collected to estimate air pressure decrease 16a. The rider enters the minimum proper pressure into the application. If the minimum proper pressure is not indicated, from the Formula (1)[1], enter the weight, bicycle weight, and tire width to calculate the minimum proper pressure. There is a need to measure on a paved road, the same road every time. In addition, the rider does not stop from the start of the measurement to the end. When the measurement start button is pressed, the application starts acquiring data. In this application, the sampling frequency for acceleration and gravity acceleration is 40 Hz. The sampling frequency for Sampling location and barometric pressure is 1 Hz. When the bicycle riding is finished, the rider presses the measurement end button. Enter the current air pressure. The application calculates the riding speed from the location information. The feature values are acquired in the interval from the time when the riding speed first reaches 5 km/h or more to the time when the riding speed last reaches 5 km/h or less. The standard deviation of acceleration on the y-axis and the amplitude spectrum for each frequency are acquired as the feature values. Gravity acceleration and barometric pressure will be used to determine the location of feature extraction.

When a certain amount of data is collected, the application becomes in an estimation state where it estimates the air pressure and judges whether it is in a dangerous condition 16b. When the number of feature data above the minimum proper pressure reaches 10 and the number of feature data below the

Table 5: Correct rate of each feature in the regression

Used feature values		Correct rate(%)
acceleration standard deviation	amplitude spectrum for each frequency	RF
○	○	77.8
○		69.4
	○	79.2

Table 6: Recall rate of each feature in the classification

Used feature values		Recall rate(%)	
Acceleration standard deviation	Amplitude spectrum for each frequency	SVM	RF
○	○	91.1	83.6
○		69.9	62.4
	○	86.5	83.6

Table 7: Recall rate of each feature in the regression

Used feature values		Recall rate(%)
Acceleration standard deviation	Amplitude spectrum for each frequency	RF
○	○	96.1
○		79.4
	○	96.1

minimum proper pressure reaches 10, the state changes to an estimation state in which air pressure decrease is estimated. When the measurement is finished in the estimation state, the estimated air pressure is displayed. In addition, if the estimated air pressure is less than the minimum proper pressure, the display prompts the rider for inflation. The estimated air pressure is estimated from three sets of data. The application displays the average of the estimated air pressure.

In the future of the application, there are several issues such as bicycle riding estimation, extraction of suitable riding locations for measurement, and operation verification. The application should be able to estimate whether the rider is riding a bicycle and can automatically measure it. Currently, the measurement is started by pressing the measurement start button and finished after pressing the measurement end button. The rider can start and finish the measurement without opening the application screen. In addition, the application should be able to automatically extract suitable locations for measurement. Currently, the rider decides on a location that can be paved and does not have to stop midway. The application should be able to automatically extract suitable locations for estimation from driving data. Finally, there is a need to encourage other people to use the bicycles.

Table 8: Setting of Evaluation Experiment 2

Number of subjects	1
Sensing terminal	Galaxy Note 9
Sampling frequency	400 Hz
Number of locations	3
Number of bicycles	3
Air pressure	150 kPa to 300 kPa
Number of data	48
Evaluation index	Correct and recall

(a) Location B **(b)** Location C

Figure 13: Location used for Evaluation Experiment 2

(a) Bicycle Y

(b) Bicycle Z

Figure 14: Bicycle used in Evaluation Experiment 2

6 CONSIDERATION OF EVALUATION EXPERIMENT

From the results of Evaluation Experiment 1, it was confirmed that the standard deviation of acceleration in the y-axis direction and the amplitude spectrum for each frequency could be used to estimate whether the air pressure was below the minimum proper pressure with a certain degree of accuracy by classification and regression. The regression was as accurate as the classification. The regression can acquire numerical results of the estimation. Numerical values provide more evidence for inflation. Therefore, regres-

Table 9: Information on the bicycles used in the Evaluation Experiment 2

Bicycles	Weight	Tire width	Minimum proper pressure
Y	24.6kg	37mm	240kPa
Z	19.6kg	37mm	230kPa

Table 10: Scores for each location and bicycle when training data is diverted at Location A, Bicycle X

Location	Bicycle	Correct rate (%)	Recall rate (%)
A	X	77.8	96.1
A	Z	75.0	50.0
B	X	62.5	100.0
C	Y	62.5	50.0
C	Z	50.0	25.0

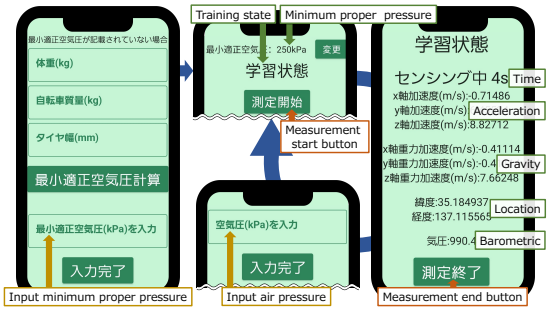

(a) Training state

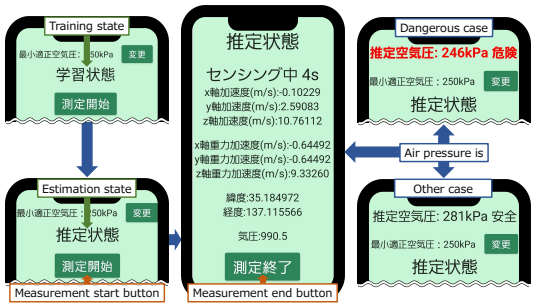

(b) Estimation state

Figure 15: Flow of application screen using the proposed method

sion using Random Forest is used for air pressure decrease estimation. The accuracy was higher when only the amplitude spectrum of each frequency was used and when both the acceleration standard deviation and the amplitude spectrum of each frequency were used as features. As shown in the Fig. 8,9, each of the feature values changes depending on the air pressure decrease. The acceleration standard deviation is affected by large bumps. The amplitude spectrum shows how much amplitude is present at each frequency. There are bumps and flat places while riding. Basically, there are many flat places. The amplitude of frequencies occurring on flat places is higher and is less affected by bumps. Therefore, two features are used for air pressure decrease estimation. The estimation could be conducted with a certain degree of accuracy even when data from different riders were used for training. Therefore, it was confirmed that the air pressure estimation was possible for the same and locationthe same bicycle.

From the results of the Evaluation Experiment 2, the recall was high in the case of a different location from the training data and the same bicycle, but in other conditions, the correctness and recall were lower than those of the same location as the training data and the same bicycle. Therefore, it was not possible to estimate air pressure decrease with high accuracy. The reason for both the correct and recall rates of Evaluation Experiment 2 may be the different structure of the bicycles. It is considered that different bicycle structures transmit vibration differently, and that the characteristics of the vibration obtained in Evaluation Experiment 1 differed from those obtained in Evaluation Experiment 2. The recall of the training data and the case of another location and the same bicycle was high, so it was found that the bicycles could be judged out of proper at the proper time, but they could be safe to travel in a safe condition. There are places that are frequently used by users and bicycles that need to be learned in advance if the current estimation method is to be implemented as an application. However, if learning is required prior to use, it is time consuming and contrary to the purpose. Therefore, there is a need to come up with learning methods without time consuming.

7 CONCLUSION

In this study, we focus on air pressure inspection and propose a method for estimating bicycle air pressure decrease based on vibration sensing using smartphone. The acceleration in the direction perpendicular to the ground is acquired with a smartphone, and the standard deviation and the amplitude spectrum of each frequency are used as features to estimate the air pressure decrease using random forests and other methods. Evaluation experiments were conducted to classify whether the best timing for tire inflation, to estimate the air pressure value and classify it based on that value, and to evaluate whether the training data from other locations and bicycles can be diverted. The results of the evaluation experiments showed that 96.1% correctly classified when tire inflation was needed, but it was difficult to divert the training data. We developed an application that promotes air pressure inspection using the proposed method.

In the future of air pressure decrease estimation, there is a need to consider a estimation method without time consuming. In this estimation method, there is a need to have riders train in advance at locations and bicycles that they frequently use. Therefore, there is a need to consider methods that do not need to be trained in advance. The machine learning algorithm used in this study required supervised data. However, there are machine learning algorithms that do not use supervised data. If the machine learning algorithms that do not need supervised data are used, there is no time consuming to train it. Therefore, we consider an unsupervised algorithm for estimating air pressure decrease. There is a need to develop and evaluate an application that can estimate air pressure decrease.

REFERENCES

[1] au Insurance. survey on bicycle inspection and equipment. https://www.au-sonpo.co.jp/corporate/news/detail-287.html. (reference 2023-11-03).

[2] Bicycle Association. bicycle safety check. https:

//baa-advisor.com/safety/safety.html. (reference 2023-11-03).
[3] A. Martinelli, M. Meocci, M. Dolfi, V. Branzi, S. Morosi, F. Argenti, L. Berzi, and T. Consumi, ”Road Surface Anomaly Assessment Using Low-Cost Accelerometers: A Machine Learning Approach, ”Sensors 2022, vol. 22, No. 10, pp. 3788 (2022).
[4] S. Roychowdhury, M. Zhao, A. Wallin, N. Ohlsson, and M. Jonasson, ”Machine Learning Models for Road Surface and Friction Estimation using Front-Camera Images, ”2018 International Joint Conference on Neural Networks (IJCNN), pp. 1-8 (2018).
[5] K. Ohara, T. Maekawa, and Y. Matsushita, ”Detecting State Changes of Indoor Everyday Objects using Wi-Fi Channel State Information, ”Proceedings of the ACM on Interactive, Mobile, Wearable and Ubiquitous Technologies, Vol. 1, Issue. 3, No. 88, pp. 1-28 (2017).
[6] X. Tang, B. Xiao, and K. Li, ”Indoor Crowd Density Estimation Through Mobile Smartphone Wi-Fi Probes, ”IEEE Transactions on Systems, Man, and Cybernetics: Systems, Vol. 50, Issue. 7, pp. 2638-2649 (2020).
[7] Kashimura. air pressure sensor. https://www.kashimura.com/goods/car/tpms/kd220.html. (reference 2023-11-03).
[8] Quarq. TyreWiz. https://www.sram.com/en/quarq/series/tyrewiz. (reference 2023-11-03).
[9] KUKiiRE. Smart Air Inflator. https://kukiire.com/. (reference 2023-11-03).
[10] Brigestone. Air Free Concept. https://www.bridgestone.co.jp/technology_innovation/air_free_concept/. (reference 2023-11-03).
[11] B. Tian, Y. Zhao, Z. Jiang, L. Zhang, N. Liao, Y. Liu, and C. Meng, ”Fabrication and Structural Design of Micro Pressure Sensors for air pressure Measurement Systems (TPMS), ”Sensors 2009, Vol. 9, No. 3, pp. 1382-1393 (2009).
[12] S. Formentin, L. Onesto, T. Colombo, A. Pozzato, S. M. Savaresi, ”h-TPMS：a hybrid air pressure monitoring system for road vehicles, Mechatronics, ”Vol. 74, 102492 (2021).
[13] R. Yamaguchi, and K. Kaji, ”Basic Study of a Method for Estimating Bicycle Air Pressure Decrease Using a Sensor in a Smartphone, ”Multimedia, Distributed, Cooperative, and Mobile Symposium2022, pp. 158-162 (2022).

(Received: November 30, 2023)
(Accepted: July 1, 2024)

Rui Yamaguchi is a graduate student at Aichi Institute of Technology. Currently, he is a graduate student of Business Administration and Computer Science, Aichi Institute of Technology. His research interests include estimating bicycle air pressure decrease.

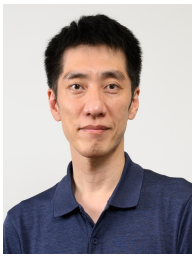

Katsuhiko Kaji received his Ph.D. in information science from Nagoya University in 2007. He became a RA at NTT Communication Science Laboratories in 2007 and an assistant professor in Nagoya University in 2010. He moved to Aichi Institute of Technology in 2015 as an associate professor, becoming a professor in 2024. His research interests include indoor positioning, human activity recognition, and human augmentation. He is a member of IPSJ.

Submission Guidance

About IJIS

International Journal of Informatics Society (ISSN 1883-4566) is published in one volume of three issues a year. One should be a member of Informatics Society for the submission of the article at least. A submission article is reviewed at least two reviewer. The online version of the journal is available at the following site: http://www.infsoc.org.

Aims and Scope of Informatics Society

The evolution of informatics heralds a new information society. It provides more convenience to our life. Informatics and technologies have been integrated by various fields. For example, mathematics, linguistics, logics, engineering, and new fields will join it. Especially, we are continuing to maintain an awareness of informatics and communication convergence. Informatics Society is the organization that tries to develop informatics and technologies with this convergence. International Journal of Informatics Society (IJIS) is the journal of Informatics Society.

Areas of interest include, but are not limited to:

- Internet of Things (IoT)
- Smart Cities, Communities, and Spaces
- Big Data, Artificial Intelligence, and Data Science
- Network Systems and Protocols
- Computer Supported Cooperative Work and Groupware
- Security and Privacy in Information Systems
- Intelligent Transportation System
- Distributed Computing
- Multi-media communication
- Information systems
- Mobile computing
- Ubiquitous computing

Instruction to Authors

For detailed instructions please refer to the Authors Corner on our Web site, http://www.infsoc.org/.

Submission of manuscripts: There is no limitation of page count as full papers, each of which will be subject to a full review process. An electronic, PDF-based submission of papers is mandatory. Download and use the LaTeX2e or Microsoft Word sample IJIS formats.

http://www.infsoc.org/IJIS-Format.pdf

LaTeX2e

LaTeX2e files (ZIP) http://www.infsoc.org/template_IJIS.zip

Microsoft Word™

Sample document http://www.infsoc.org/sample_IJIS.doc

Please send the PDF file of your paper to secretariat@infsoc.org with the following information:

Title, Author: Name (Affiliation), Name (Affiliation), Corresponding Author. Address, Tel, Fax, E-mail:

Copyright

Publisher

Address: Informatics Laboratory, 3-41 Tsujimachi, Kitaku, Nagoya 462-0032, Japan

E-mail: secretariat@infsoc.org

CONTENTS